Meteorol. Zeitschrift, N.F. 2, 51—69 (April 1993)

Land surface processes over flat agricultural terrain: A comparison of measurements and simulation using LOTREX-10E/HIBE88 data

N. KALTHOFF, G. SCHÄDLER, F. FIEDLER and G. ADRIAN

Summary. During the months of May and June, 1988 the field experiment HIBE88 (Hildesheimer Börde Experiment 1988) was carried out as a part of the LOTREX-10E programme. One major goal of this project is the determination of areally-averaged surface fluxes, which can be used for the intercomparison with results obtained from satellite data via parameterisation schemes. Since only point data are available from ground stations, it is necessary to obtain area averages.

Here we present areally-averaged surface fluxes for the different land use classes and the whole HIBE area for the 13th of June, 1988. Durig this cloudfree day, besides data from the surface stations, radiosonde and aircraft data are available. Areally-averaged energy balances are estimated for the different land use types and for the whole domain by the mesoscale model KAMM, where a soil-vegetation model is implemented. The model results are compared with the appropriate surface observations at different sites and different vegetation types. The evolution of the PBL is compared with observations from radiosonde ascents and aircraft data. The main results are:

— The observed variance of the sensible heat flux within a specific type of vegetation is low, while the variance of the latent heat flux is much higher.
— The turbulent fluxes at a specific site and land use type can well be predicted by the model.
— The modelled vertical profiles of the potential temperature and humidity as well as the inversion height agree reasonably well with radiosonde and aircraft data. The sensible and latent heat fluxes within the PBL obtained by the model are generally higher than those estimated by the aircraft data.
— According to a cluster analysis the mean diameter of the areas with uniform land use is less than 2 km. Since this is below the limit where persistent secondary circulations can be expected, the mesoscale contributions to the turbulent fluxes are low within the PBL, thus for the HIBE campaign results of the model obtained with different grid sizes yield quite similar results.

Landoberflächenprozesse über ebenem landwirtschaftlich genutztem Gelände: ein Vergleich von Messung und Rechnung unter Verwendung von LOTREX-10E/HIBE88-Daten

Zusammenfassung. Im Mai/Juni 1988 fand als Teil des LOTREX-10E-Programmes das Feldexperiment HIBE88 (Hildesheimer Börde Experiment 1988) statt. Ein Hauptziel dieses Projekts ist die Bestimmung flächengemittelter Flüsse. Diese Flüsse können als Bodenwerte zum Vergleich mit aus Satellitenmessungen erhaltenen Daten dienen. Da Bodenstationen nur Punktdaten liefern, müssen Flächenmittel bestimmt werden.

In diesem Artikel betrachten wir Flüsse, gemittelt sowohl über einzelnen Landnutzungsklassen als auch über das gesamte HIBE-Gebiet für den 13. Juni 1988. An diesem wolkenfreien Tag sind zusätzlich zu den Bodenstationsdaten auch Radiosonden- und Flugzeugmessungen verfügbar. Die Punkt- und Gebietsenergiebilanzen werden mit Hilfe des mesoskaligen Modells KAMM mit einem angekoppelten Boden/Vegetationsmodell berechnet. Die Modellergebnisse werden mit den entsprechenden Bodenbeobachtungen an verschiedenen Orten und verschiedenen Vegetationsarten und die Entwicklung der Grenzschicht wird mit Radiosonden- und Flugzeugbeobachtungen verglichen. Die wichtigsten Ergebnisse sind:

— Im Gegensatz zur viel größeren Streuung des latenten Wärmeflusses ist die Streuung des fühlbaren Wärmeflusses bei gegebener Vegetationsart gering.
— Die turbulenten Flüsse an den verschiedenen Stationen werden vom Modell gut wiedergegeben.
— Die Vertikalprofile von Temperatur und spezifischer Feuchte und die Grenzschichthöhe stimmen zufriedenstellend mit den Radiosonden- und Flugzeugdaten überein. Die vom Modell berechneten fühlbaren und lateten Wärmeflüsse sind im allgemeinen höher als die von den Flugzeugen gemessenen.
— Gemäß einer Cluster-Analyse ist der mittlere Durchmesser von Gebieten gleicher Landnutzung kleiner als 2 km. Dies liegt unterhalb der Grenze, ab der mesoskalig bedeutsame Sekundärzirkulationen erwartet werden können, daher sind die mesoskaligen Beiträge zu den Flüssen innerhalb der Grenzschicht gering. Aus diesem Grund sind die Unterschiede zwischen den Modellergebnissen, die mit den verschiedenen Gitterweiten berechnet werden, nicht groß.

1 Introduction

The transformation of the incoming radiative energy at the ground into the sensible, latent and soil heat flux drives the climatic state on all meteorological scales. In order to get these surface fluxes as input parameters on the global scale for General Circulation Models (GCM's) the use of satellite data is indispensable. Satellite data, however, a priori do not yield these required values. Thus, first it is necessary to develop algorithms to obtain surface fluxes from radiation properties and then to calibrate and validate these algorithms with ground truth data. For this intercomparison two major things have to be done:
(i) to find out the decisive physical and biophysical processes the energy transformation depends on and then to extract the relevant quantities,
(ii) to estimate from the measurements at one point areally-averaged means for the grid size of the satellite data.

Concerning (i), with the aid of soil-vegetation models e.g. PAN and MAHRT (1987), SCHÄDLER et al. (1990) or JACQUEMIN and NOILHAN (1990) the relevant parameters were identified (leaf area index, minimum stomatal resistance, vegetation cover, vegetation height, albedo, soil moisture)

DOI: 10.1127/metz/2/1993/51

Gebrüder Borntraeger Stuttgart, Germany

and thus these models in the meantime have turned out to be indispensable tools for the interpretation of observed data.

As to (ii), up to now attempts have been made to determine areally-averaged surface fluxes by measurements and/or model calculations. For example, within ISLSCP (BECKER et al. 1988) several experiments were carried out on different scales: La Crau at 50 km^2, LOTREX at 145 km^2, FIFE at 225 km^2 (SELLERS 1988) and HAPEX at 10 000 km^2 (ANDRÉ et al. 1988). BETTS et al. (1990) e. g. compared ground based measurements and budget calculations with aircraft data from the FIFE experiment. He found great discrepancies for the turbulent fluxes, especially between the surface measurements and the aircraft observations.

The calculation of areally-averaged surface fluxes by use of numerical models can be done in two different ways. The first is to resolve the area of interest in such a way that all different land use classes present are accounted for.

The second method is to find an appropriate averaging procedure for the parameters determining the surface fluxes. This was done e. g. by MAHRT (1987) and CLAUSSEN (1991), who used an effective roughness length (FIEDLER and PANOFSKY 1972) and blending height, introduced by WIERINGA (1986) and MASON (1988). A similar study was done by BELJAARS and HOLTSLAG (1991), who tested their parameterisation scheme with data from the MESOGERS-experiment (WEIL et al. 1988) and VIHMA and SAVIJÄRVI (1991), who compared several theories for the calculation of the effective roughness length with results from a mesoscale model.

In the present paper we are using the first method. This was already done for HAPEX data by ANDRÉ et al. (1990), who compared surface observations with aircraft measurements and model results. Similar to BETTS et al. (1990) they found that while the model results and the observations agree quite well the aircraft data underestimate the fluxes of sensible and latent heat.

We use the data from the HIBE88 field campaign, one activity within the LOTREX-10E concept (LOngitidunal land-surface TRaverse EXperiment 10 degrees East). The major subjects of the LOTREX-10E programme are to determine the energy balance of the earth at different longitudes (net radiation, sensible heat flux, evaportion and soil heat flux) in relation to soil (e. g. soil moisture, soil type) and vegetation characteristics (e. g. vegetation height, vegetation cover, LAI) of different land uses by simultaneous ground based and satellite measurements. Our aim is to calculate areally-averaged mean fluxes of the grid size of the satellite data and of the whole experiment domain. In order to get areally-averaged means from the point measurement we used the coupled soil-vegetations-atmosphere mesoscale model KAMM ('Karlsruhe Atmospheric Mesoscale Model').

The paper is divided in the following way: in section 2 an overview of the available data is given. Additionally we compare different methods to calculate the surface fluxes of heat and moisture. In section 3 a description of the soil-vegetation and the atmospheric model together with the initialisation procedure is given. In section 4 the results are presented: in the first part the model simulations for the PBL, concerning inversion height, potential temperature-, humidity- and flux profiles are compared with aircraft measurements and data from the radiosonde ascents. In the second part the turbulent fluxes of the model for different land uses are compared with observations. The influence of the grid size of the model calculations on the mean fluxes is studied. Furthermore the variability of the meteorological parameters within the whole area (with its different land uses) and within each land use class is estimated and compared with the measured variability.

2 Available data

2.1 Land use

The HIBE88 experiment took place in the Hildesheimer Börde (FRG), from 29 May until 23 June 1988. The area is a rather flat plain about 80—100 m above MSL and about 12 km in diameter located in the southeast of Hannover (Fig. 1).

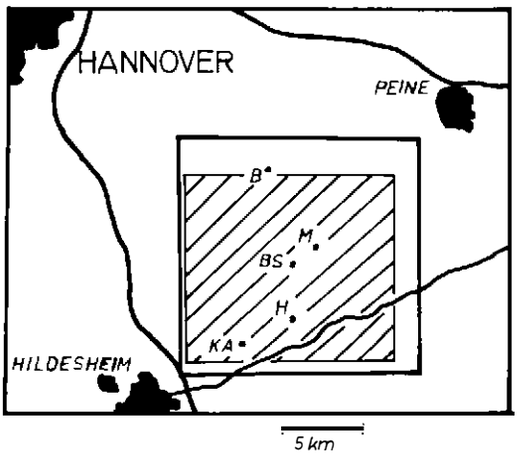

Fig. 1. The 'Hildesheimer Börde' area where the HIBE88 campaign took place. The experimental domain is marked by the outer box, the simulation domain is hatched. The station of Berlin is marked by B, of Braunschweig by BS, of Hannover by H, of Karlsruhe by KA and of München by M.

Abb. 1. Das Gebiet der Hildesheimer Börde, in dem das HIBE88-Experiment stattfand. Das Experimentgebiet ist durch den äußeren Rahmen gekennzeichnet, wohingegen das Rechengebiet schraffiert dargestellt ist. Die Stationen sind wie folgt bezeichnet: Berlin: B, Braunschweig: BS, Hannover: H, Karlsruhe: KA, München: M.

Within this area several energy balance stations were installed. A more complete desription of the whole experiment is given by HOPPMANN and HOFFMANN (1991). A detailed description of the station and the measurements of the group of Karlsruhe is given by KALTHOFF et al. (1991).

Here only a brief description of available data is given, as far as we refer to them for the initialisation of or for the intercomparison with the model.

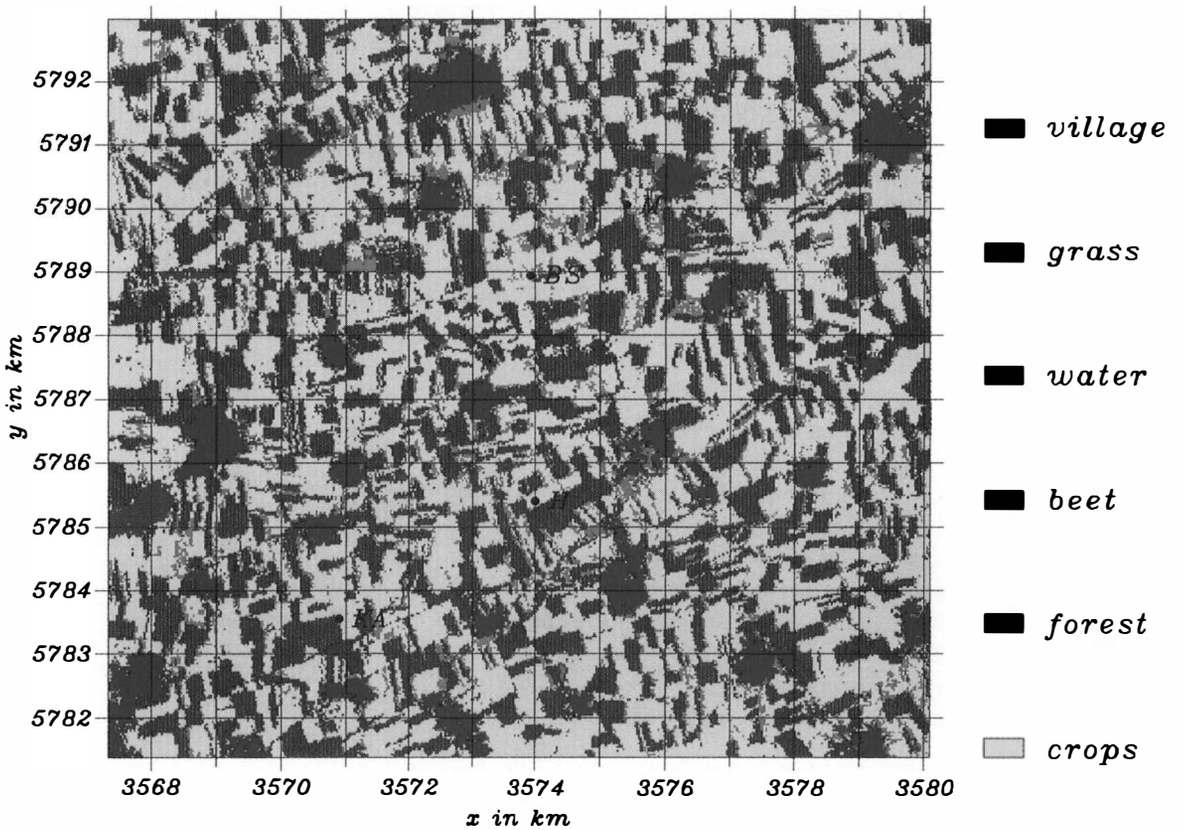

Fig. 2. Map of the land use classification of the Hildesheimer Börde as obtained by LANDSAT; the resolution is 30 × 30 m.

Abb. 2. Landnutzungskarte nach einer LANDSAT-Aufnahme; die Auflösung beträgt 30 × 30 m.

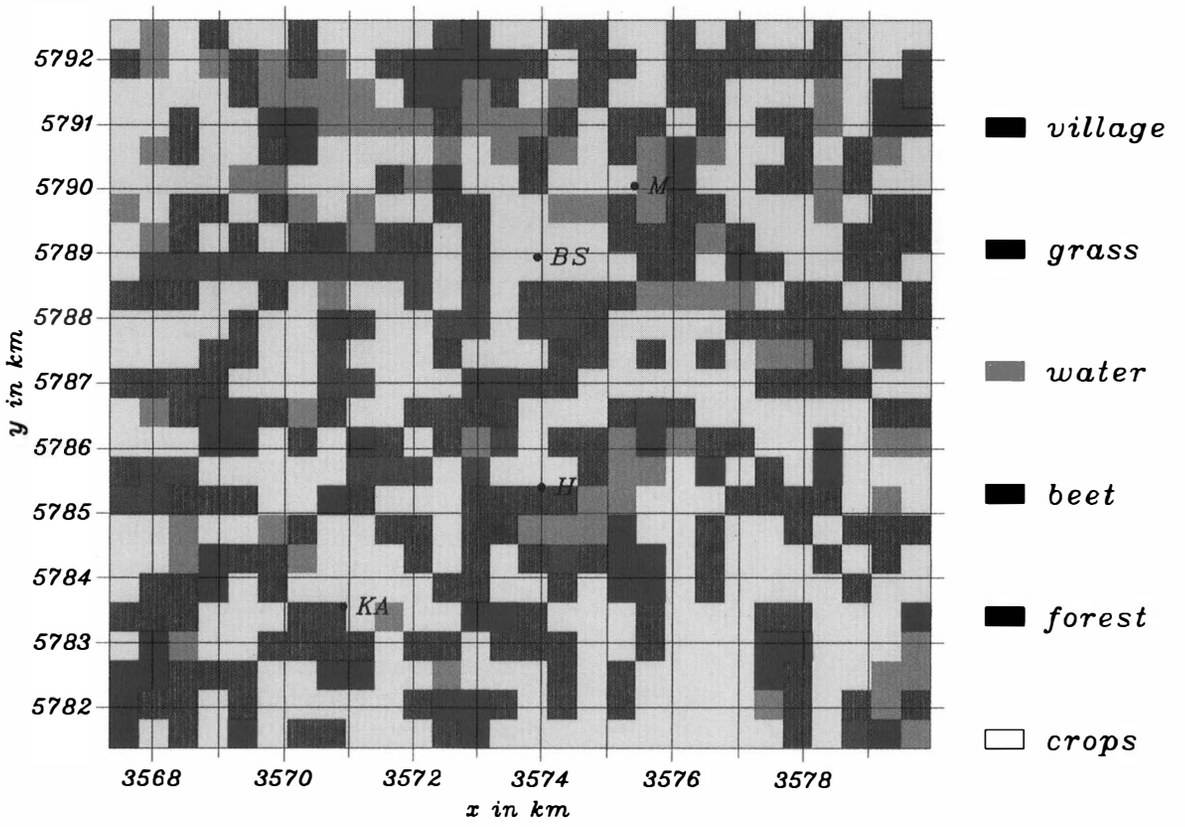

Fig. 3. Land use classification for model grid size of 450 × 450 m as obtained by the method described in the text.

Abb. 3. Landnutzungsklassen für eine Modellgitterweite von 450 × 450 m entsprechend dem im Text beschriebenen Verfahren.

The soil consists of loam, 2 meters in thickness. The uppermost layer (60—70 cm) consists of pseudogley chernozem.

The land use data were derived from LANDSAT data for a grid size of 30 m by 30 m estimated by the group of Braunschweig (LÖPMEIER et al. 1991), where 19 types of land use classes were distinguished. We reduced the number of land use classes to 6 by collecting e.g. the different kinds of crops (wheat, barley, rye) or forests (coniferous, deciduous and mixed forest). In Figure 2 the map of the land use of the modelling domain is given with the original LANDSAT resolution of 30×30 m.

Since we want to run the mesoscale model with different grid sizes, and each gridpoint has to be assigned only one land use class we have to find a way to obtain the land use on a coarser grid from the land use distribution on a finer grid, where the starting grid is the LANDSAT scene with reduced number of land use classes. In order to make the results from the different model runs intercomparable we require that the percentage of the land use classes remains approximately constant for the whole model domain independent of the grid size and apply a majority rule to arrive at the coarser grid. The details of the method are described below.

The six land use classes are denoted by L_λ. The fine grid is assumed to have m × n points, numbered with indices i, j, and the class at point (i, j) is denoted by c_{ij} with $c_{ij} \in \{L_1, ..., L_6\}$. Similarly we have C_{IJ} on the coarser grid, I = 1, ..., M, J = 1, ..., N. Each grid element of the coarser grid is assumed to contain $m_c \times n_c$ elements of the finer grid. To obtain C_{IJ}, we define

$$C_\lambda = \sum_{i=1}^{m_c} \sum_{j=1}^{n_c} c_{\lambda ij}$$

with

$$c_{\lambda ij} = \begin{cases} 0, & c_{ij} \neq L_\lambda \\ 1, & c_{ij} = L_\lambda \end{cases}$$

The summation is over all fine grid elements contained in the coarse grid element. The $C_{\lambda IJ}$ on the coarser grid are obtained in the same way as $c_{\lambda ij}$. Now we obtain C_{IJ} by the majority rule $C_{IJ} = \lambda_0$, with $C_{\lambda_0} = \max_\lambda \{C_\lambda\}$. However, with this algorithm the relative percentage in general is not constant for the different land use classes, i. e.

$$\sum_{i=1}^{m} \sum_{j=1}^{n} c_{\lambda ij} \neq \sum_{I=1}^{M} \sum_{J=1}^{N} C_{\lambda IJ}.$$

We therefore introduce weighting factors g_λ in the land use classes:

$$\tilde{C}_\lambda = g_\lambda \sum_{i=1}^{m_c} \sum_{j=1}^{n_c} c_{\lambda ij},$$

and determine the g_λ in such a way that

$$\sum_{i=1}^{m} \sum_{j=1}^{n} c_{\lambda ij} \approx \sum_{I=1}^{M} \sum_{J=1}^{N} \tilde{C}_{\lambda IJ}.$$

where the $\tilde{C}_{\lambda IJ}$ are obtained in the same way as the $C_{\lambda IJ}$. Since *max* is a nonlinear operator, the g_λ have to be determined iteratively. Of course, no strict equality can be achieved, since e. g. small and sparse water surfaces drop out.

The weighting factor can be interpreted physically. It will be low if the different areas of a specific land use cling together and/or if they are concentrated at a specific site, whereas it will be high if the converse is true. For example, grass, which is spread in small patches over the whole area, necessitates a weighting factor larger than 1 to maintain the original percentage coverage. The weighting factors together with the percentages are given in Table 1 for the original LANDSAT scene and for 450 and 990 m grid. As can be seen the percentage coverage of the different land use classes nearly remains constant independent of the chosen grid size.

Table 1. Percentage coverage p and weighting factors g.

Tabelle 1. Prozentuale Anteile p und Gewichtsfaktoren g.

class	p_0	p_{450}	p_{990}	g_{450}	g_{990}
crops	47.2	45.7	46.9	0.8	0.79
forest	5.1	4.7	4.5	2.25	2.075
beet	29.2	30.2	29.5	1.05	1.082
water	0.1	0.1	0.0	1.0	1.2
grass	10.0	10.8	10.6	2.25	2.52
village	8.4	8.3	8.3	1.0	1.2

In Figure 3 the map of the land use is given for the grid size of 450×450 m according to the algorithm. The land use classes of 450×450 m and 990×990 m grid size are taken for the calculations of the mesoscale model in section 4.

2.2 Surface layer and soil measurements

All meteorological data measured at the different sites are available as ten minutes means. At the station of Karlsruhe KA at both the sugar-beet and the wheat field the following instrumentation was installed: albedometers were used to detect the shortwave up- and downward radiation, radiometers were used to receive the up- and downward components of the short- and longwave radiation. The turbulent fluxes of sensible and latent heat were measured by an ultrasonic anemometer-thermometer and a Lyman-α hygrometer. Heat flux plates were taken to obtain the soil heat flux.

The temperature, humidity and wind speed were measured at the heights of 0.5, 1.0, 2.0, 4.0, 8.0 and 16 m. The wind direction was measured at 18 m height. An infrared-thermometer (8—14 μm wavelength) was used to get the surface temperature. The soil temperature is available only in the sugar-beet field at 1, 2, 4, 8, 16, 32 and 64 cm depth.

At the station of Braunschweig BS temperature-, humidity- and wind speed profiles as well as the components of the radiation balance are available. The soil temperature was measured at the depth of 2 and 10 cm. Additionally the group of Braunschweig performed radiation temperature measurements over different surfaces several times a day.

At the station of Hannover H, where masts were erected on a sugar-beet field and on a wheat field (LINSE and TETZ-

LAFF 1991), for that day only the wind-, temperature-, and humidity profiles are available (generally at two heights).

At a sugar-beet field (site M) and the wheat field (site BS) the soil water content is given. These measurements have been done by the groups of Freiburg by a microwave-sonde at the depths of 1, 2, 4, 7 and 14 cm and by a neutron probe between soil surface and 60 cm depth, described by WEGEHENKEL and MAUSER (1991) and by the group of Bochum by the carbid- and gravimetric methods (NEUMANN and SCHULTZ 1991) between the soil surface and 1 m depth.

2.3 Surface fluxes as obtained by different methods

During HIBE88 different techniques were used to estimate the turbulent fluxes of sensible H and latent heat E. Since at the station of Karlsruhe KA the eddy-correlation measurements and the measurements of the temperature, humidity- and wind speed profiles were carried out simultaneously the results of the different techniques can be compared best at that site.

To obtain the turbulent fluxes from the profiles two aerodynamic methods are tested. By the first (I) the turbulent fluxes are given by:

$$H = -\rho c_p \kappa^2 (z - d)^2 \frac{\partial u}{\partial z} \frac{\partial T}{\partial z} (\phi_H \phi_M)^{-1}, \quad (1)$$

and

$$E = -\rho L \kappa^2 (z - d)^2 \frac{\partial u}{\partial z} \frac{\partial q}{\partial z} (\phi_H \phi_M)^{-1}, \quad (2)$$

with the integrated stability functions ϕ_M and ϕ_H adopted from OKE (1987):

$$(\phi_H \phi_M)^{-1} = (1 - 5Ri)^2 \quad \text{for } Ri \geq 0, \quad (3)$$

and

$$(\phi_H \phi_M)^{-1} = (1 - 16Ri)^{3/4} \quad \text{for } Ri < 0, \quad (4)$$

where ρ is the air density, c_p is the specific heat at constant pressure, u is the horizontal wind speed, Ri is the gradient Richardson number, d is the displacement height, and κ is the von Kármán constant ($\kappa = 0.4$).

The second method (II) is described by NIEUWSTADT (1978). There

$$H = -\rho c_p u_* T_*, \quad (5)$$

and

$$E = -\rho L u_* q_*. \quad (6)$$

Using the wind speed u_i, the temperature T_i and the specific humditiy q_i measured at three heights we computed the functions

$$f_u = \sum_{i=1}^{3} (u_i - u_{Bi})^2, \quad (7)$$

$$f_T = \sum_{i=1}^{3} (T_i - T_{Bi})^2, \quad (8)$$

$$f_q = \sum_{i=1}^{3} (q_i - q_{Bi})^2. \quad (9)$$

u_{Bi}, T_{Bi} and q_{Bi} are the values of the wind speed, temperature and humidity calculated by using the empirical profile functions of BUSINGER et al. (1971). The parameters of u_*, T_* and q_* are found from the condition that the functions

$$F_H = g_u f_u + g_T f_T \quad (10)$$

and

$$F_E = g_u f_u + g_q f_q \quad (11)$$

attain a minimum. The weighing factors g_u, g_T and g_q are defined by $g_u = 1/\Delta u^2$, $g_T = 1/\Delta T^2$ and $g_q = 1/\Delta q^2$; here they are set to one. The main differences of the two methods result from the fact that in method I the profiles of the temperature, wind speed and humditiy are fitted separately whereas in method II the fits of the three profiles are done simultaneously under the constraints given by equations (10) and (11).

Results for the station of Karlsruhe KA for the 13th of June are shown in Figure 4 for the sugar beets and in Figure 5 for the wheat. It can be seen that the results from the two aerodynamic methods agree well among themselves for sugar beet and for wheat. The agreement between the aerodynamic methods and the eddy-correlation method is good for the sugar beet, whereas for the wheat, although the maxima of H and E at noon are well reproduced, the sensible heat flux is underestimated during the afternoon and the latent heat flux is underestimated during the morning.

Both aerodynamic methods were applied to the wheat field at the site of BS and coincide quite well, too. We decided to use the first aerodynamic method (I) for the comparison of the measurement with the model results, because with this method the residuum for the energy balance over all sites is smaller.

2.4 PBL data

Radiosonde ascents have been performed at the station of KA during the 13th of June at 8:30, 11:00, 14:00, 18:00 and 20:00 CEST, where temperature, humidity, wind speed and wind direction were measured. As northeasterly winds dominate during the day (see Fig. 7), the air travels over most of the HIBE domain, before it reaches the radiosonde station. Thus a good adjustment of the air flow to the underlying surface is given up to about 1000 m, if an internal boundary layer slope of about 0.1 (HANNA 1987) is assumed and hence the radiosonde data of the PBL can be considered as representative for the HIBE domain.

During the 13th of June the group of the DLR Oberpfaffenhofen performed measurements of the meteorological parameters of temperature and humidity, as well as of the turbulent fluxes in the PBL by the Falcon, the Queen Air aircrafts and motorgliders. A detailed description of their intrumentation, flight pattern and results are given by RÖSLER and JOCHUM (1988) and JOCHUM et al. (1991). A comparison of PBL characteristics of the aircraft data with 3D-model simulations is described by GRAF and SCHUMANN (1991).

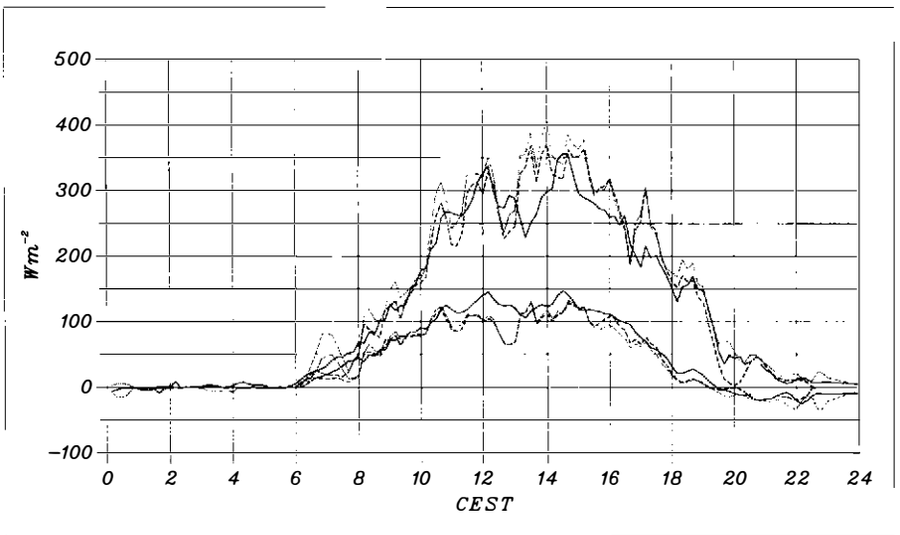

Fig. 4. Intercomparison of the turbulent fluxes for the sugar-beet field at site KA, obtained by different methods for 13th of June, 1988. The upper curves show the latent heat flux, the lower curves the sensible heat flux. The solid line indicates the eddy-correlation measurements, the dashed line gives the results of the aerodynamic method (I) (Eqns. (1) and (2)). The dotted line shows the fluxes according to the aerodynamic method (II) (Eqns. (5) and (6)).

Abb. 4. Vergleich der mit verschiedenen Methoden über Zuckerrüben an der Karlsruher Station erhaltenen turbulenten Flüsse für den 13.6.88. Die oberen Kurven zeigen den latenten Wärmefluß, die unteren den fühlbaren. Die durchgezogene Kurve gibt die Messungen nach Korrelationsmethode wieder, die strichlierte die Ergebnisse der aerodynamischen Methode (I) (Gln. (1) und (2)). Die punktierte Kurve zeigt die Flüsse nach der aerodynamischen Methode (II) (Gln. (5) und (6)).

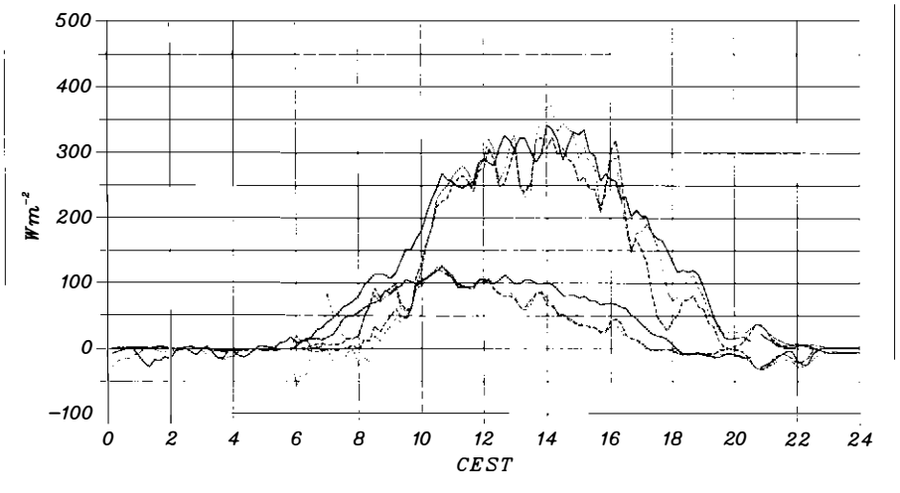

Fig. 5. Same as Figure 4, but for the wheat field at site KA.

Abb. 5. Wie Abb. 4, aber für Weizen an der Karlsruher Station.

3 Model description and initialisation

3.1 Atmospheric model

The atmospheric part of the model (henceforth abbreviated to AM) is the three-dimensional nonhydrostatic mesoscale model KAMM. This model has been described recently by ADRIAN and FIEDLER (1991), so that we can limit ourselves to pointing out the differences between the model version used here and the version described in that paper.

Turbulent diffusion is calculated using the eddy viscosity concept, with the gradient Richardson number as argument of the stability functions throughout the atmosphere. During the simulations it turned out that accounting for cooling of the atmosphere due to the divergence of longwave radiation was essential for obtaining realistic results; therefore the radiation scheme described in SCHÄDLER (1990) and based on the work of HOUGHTON (1979) and STALEY and JURICA (1970) is used to calculate the longwave radiative fluxes. The attenuation of solar radiation due to different absorbers and scatterers is computed using a formulation given by ATWATER and BROWN (1974).

3.2 Soil-vegetation model

The soil-vegetation model (henceforth abbreviated as SVM) is the one described in SCHÄDLER et al. (1990), except that

Table 2. Parameters for the vegetation model.

Tabelle 2. Parameter des Vegetationsmodells.

LAI is the leaf area index, σ_f is the vegetation cover, R_0 (s/m) is the minimum stomata resistance, ST is the stem fraction, z_{root} (m) is the mean root depth, d (m) is the displacement height, z_0 (m) is the roughness length, α_f is the vegetation albedo, ϵ_f is the vegetation emissivity.

parameter	water	grass	forest	villages	beets	crops
LAI	—	1.0	6.0	1.0	2.2	5.3
σ_f	—	0.7	0.9	0.3	0.45	0.7
R_0	—	250.	250.	2000.	180.	180.
ST	—	1.5	1.5	3.0	1.1	1.1
z_{root}	—	0.1	>0.6	—	0.3	0.50
d	0.	0.1	5.0	2.0	0.16	0.58
z_0	0.005	0.03	0.50	0.50	0.02	0.09
α_f	—	0.2	0.12	0.15	0.16	0.2
ϵ_f	—	0.96	0.95	0.90	0.95	0.96

the factor 1/0.74 in the formula for q_* is retained. The coupling between the SVM and the atmospheric model (AM) is done via the prognostic variables in the lowest and second lowest layer of the AM: the lowest model layer is assumed to lie within the vegetation layer and the second lowest model layer is assumed to lie within the Prandtl layer of the atmosphere. As mentioned above the AM provides the downward shortwave and longwave radiative fluxes for the SVM. The parameters needed for the different land use classes of the SVM are listed in Table 2. Most of the parameters for wheat and sugar beet were obtained from measurements at KA, the other ones are taken from the literature (WILSON et al. 1987, DICKINSON et al. 1986).

3.3 Initialisation of the model

The initialisation of the model as a whole involves three steps:
— prescribing the (steady) basic state of the AM
— prescribing initial values for the AM
— prescribing initial values for the SVM
These steps will now be described in turn.

3.3.1 Basic state of the atmospheric model

The formulation of the AM requires the splitting of the Exner function π and the potential temperature θ into a basic state part π_g resp. θ_g and a mesoscale deviation π' resp. θ'. The basic state parts have to satisfy the geostrophic relations:

$$\frac{\partial \pi_g}{\partial x} = \frac{f\, v_g}{c_p \theta_g} \tag{12}$$

$$\frac{\partial \pi_g}{\partial y} = -\frac{f}{c_p}\frac{u_g}{\theta_g} \tag{13}$$

$$\frac{\partial \pi_g}{\partial z} = -\frac{g}{c_p}\frac{1}{\theta_g} \tag{14}$$

where u_g and v_g are the components of the geostrophic wind vector. These functions may vary in space (especially in the vertical), but not in time. Given vertical profiles of u_g, v_g and θ_g at a specific point (x_0, y_0) as well as $\pi_g(x_0, y_0, z = 0)$, the ansatz

$$\pi_g(x, y, z) = a(z) + b(z)\,(x - x_0) + c(z)\,(y - y_0) \tag{15}$$

allows for a unique solution for the functions a, b, c, i. e. the field $\pi_g(x, y, z)$ is determined. Then from the geostrophic relations the functions u_g, v_g and θ_g can be calculated. We used radiosonde data from the Karlsruhe station KA averaged over six ascents from 20:00 on 12.6.88 to 18:00 on 13.6.88 as an approximation to $u_g(x_0, y_0, z)$, $v_g(x_0, y_0, z)$ and $\theta(x_0, y_0, z)$. x_0 and y_0 were chosen to lie in the center of the model domain.

3.3.2 Initial values for the atmospheric model

In addition to the basic state, the AM needs initial values for its prognostic variables u, v, θ, q. We let the simulation start at 20:00 on 12.6.88 and took radiosonde data from that time to initialise potential temperature and specific humidity. We used the results of a one-dimensional model run for 24 hours with the same basic state as the three-dimensional model to initialise the horizontal wind (same profile in the whole domain). Figure 6 a and b give the initial profiles for wind, potential temperature and humidity on the vertical grid of the model.

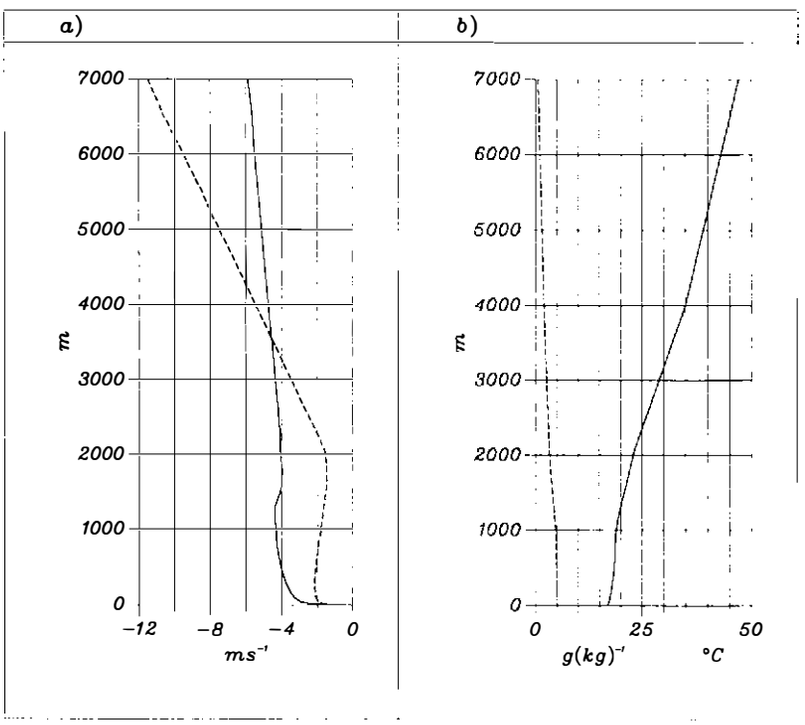

Fig. 6. Vertical profiles used for the initialisation of the mesoscale model for the 13th of June, 1988; a) wind components (solid: WE component, dashed: SN component), b) potential temperature (solid) and specific humidity (dashed). The data have been obtained from the radiosonde ascents at site KA.

Abb. 6. Vertikalprofile der zur Modell-Initialisierung verwendeten Größen für den 13.6.88; a) Windkomponenten (durchgezogen: WE-Komponente, strichliert: SN-Komponente), b) potentielle Temperatur (durchgezogen) und spezifische Feuchte (strichliert). Die Daten wurden aus Radiosondenaufstiegen an der Karlsruher Station gewonnen.

3.3.3 Initial values for the SVM

The seven computational levels of the soil model are placed in 1, 2, 4, 8, 16, 32 and 64 cm depth. To initialise the soil temperatures under the sugar beet we took the temperatures measured at KA. For crops we used the temperatures measured in 2 and 10 cm depth at BS, and extrapolated them according to a typical soil temperature profile under wheat (measured during HIBE89 at the Karlsruhe site under similar conditions). For the soil water content we employed microwave data obtained by the Freiburg group obtained at the site M (beet) and site BS (wheat). For the deeper layers we used available gravimetric and neutron-sonde data. For the soil temperatures and water contents under forest and villages, we used guessed values and adjusted them by running a one-dimensional model for 24 hours; the initial soil data for grass were the same as those for beet.

The soil type used was sandy loam as parameterised in CLAPP and HORNBERGER (1978); for villages we used the same parameters except for reduced hydraulic and thermal conductivity (and reduced initial soil water content). Tables 3 and 4 list the initial values of soil temperature and soil water content for the different land use classes.

Table 3. Initial soil temperature profiles (degrees Celsius).

Tabelle 3. Anfangsprofile der Bodentemperatur (Grad Celsius).

depth (cm)	water	grass	forest	villages	beet	crops
1	15.	16.3	16.6	26.0	16.3	15.8
2	15.	16.6	16.5	27.0	16.6	15.4
4	15.	16.5	16.2	28.0	16.5	15.1
8	15.	16.8	15.6	28.0	16.8	14.5
16	15.	15.9	14.4	22.4	15.9	13.7
32	15.	14.1	13.0	14.0	14.1	13.0
64	15.	13.3	13.0	13.3	13.3	12.5

Table 4. Initial soil water content profiles (m^3/m^3).

Tabelle 4. Anfangsprofile des Bodenwassergehalts (m^3/m^3).

depth (cm)	water	grass	forest	villages	beet	crops
1	1.	0.26	0.31	0.08	0.26	0.33
2	1.	0.27	0.31	0.09	0.27	0.35
4	1.	0.28	0.31	0.1	0.28	0.40
8	1.	0.31	0.31	0.1	0.31	0.33
16	1.	0.29	0.31	0.1	0.29	0.35
32	1.	0.28	0.32	0.1	0.28	0.29
64	1.	0.28	0.35	0.1	0.28	0.29

4 Results

June 13 was chosen for the intercomparison of model results and observations, because this day was one of the few nearly cloudless days. Additionally on this day aircraft measurements were performed and radiosonde ascents were carried out with a higher temporal resolution than usual.

The synoptic situation was characterised by a high pressure system centered in the south of Great Britain leading to calm winds (about 2 ms^{-1} at 4 m height). During the day, a low pressure system centered over North Scandinavia moved south-eastward. The warm air of this low pressure system striked Northern Germany, indicated at the KA site by a drop of the surface pressure, passing of clouds, reduced global radiation and a change of wind direction from NNE to NNW between 16:00 CEST and 18:00 CEST. This is illustrated in Figure 7, where the observed diurnal variation of pressure, global radiation, wind speed and wind direction at the wheat field of the KA site is shown.

4.1 PBL characteristics

In this section we are presenting the results of the simulations and compare them with measured data where possible. The calculations were done with the three-dimensional model in two modes: i) in the one-dimensional mode with the 990 m grid, with no horizontal coupling of the model variables (denoted by L0), and ii) in the fully three-dimensional mode for grid sizes 450 m (L450) and 990 m (L990). All simulations were run with a time step of 15 s.

It is interesting to consider beforehand what differences between those two modes can be expected. The main difference between the one dimensional and the three dimensional mode is that the latter admits the possibility of secondary circulations due to differential heating; this might alter the development of the PBL as a whole, the ratio of the subgrid scale to the resolved fluxes, the meteorological quantities near the ground and the energy balance at the grid points. For such secondary circulations to arise, we must have low wind speeds and sufficiently large adjacent areas with sufficiently large temperature differences. In the case of lake breezes, this requirement was quantified by BIGGS and GRAVES (1962), who introduced a lake breeze index $LB = U^2/(c_p \Delta T)$, where U is the wind speed and ΔT is the difference between the maximal air temperatures over land and the surface water temperature of the lake. Wind and air temperature are taken from routine measurements at meteorological stations. They found that a lake breeze is likely to occur when $LB < 0.003$. If we adopted this criterion for the present case with $U \approx 4$ m/s we would need $\Delta T \approx 10$ K. Such horizontal temperature differences did not occur. The second requirement, namely that the areas with different temperatures must be sufficiently large, seems more serious. We performed a cluster analysis of the land use distribution for the 990 m and 450 m grids. The method used was the one by HOSHEN and KOPELMAN (1976) as described by GOULD and TOBOCHNIK (1988). The results are shown in Table 5, where *a* and *m* are the average and the maximum cluster size, both in km.

We note that there is a connection between the cluster size and the weighting factors introduced in section 2: small cluster size indicates a sparse and incoherent distribution of the particular land use class which necessitates a higher weighting factor. In an analysis of secondary circulations induced by periodic strips of different soil water content (i.e. different surface temperature), SCHÄDLER (1990) found that such strips must have an extension of about

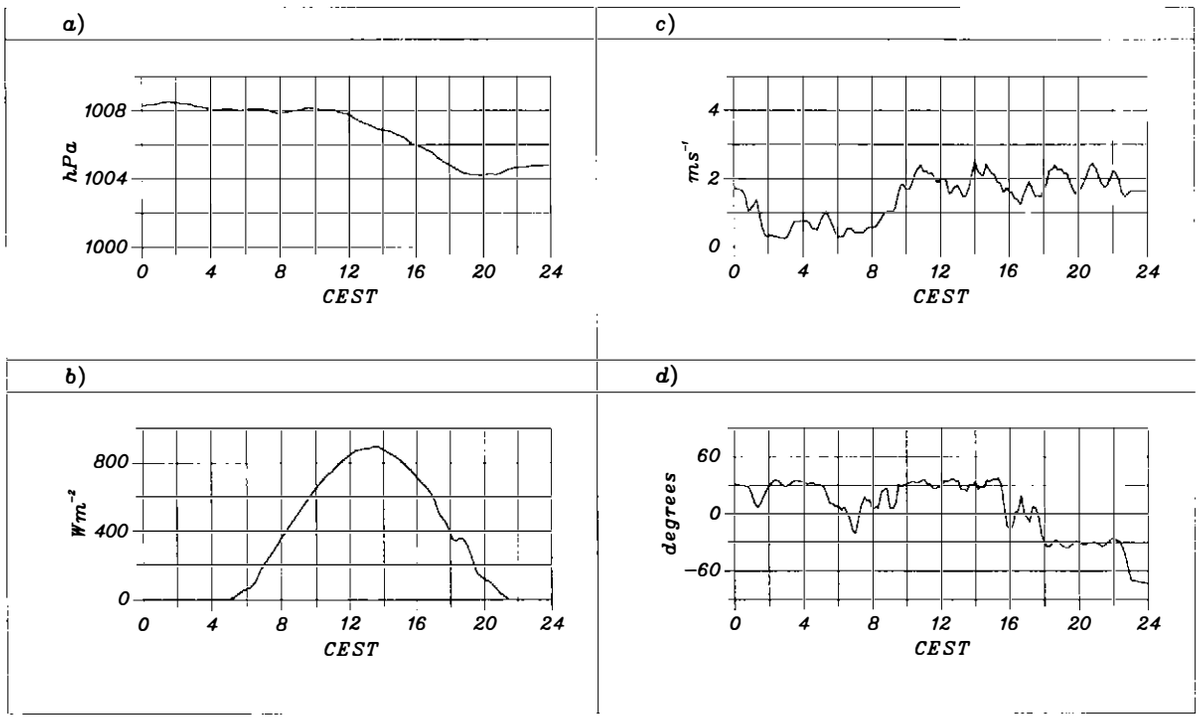

Fig. 7. Thirty-minute mean values of surface pressure (a), global radiation (b), wind speed (c) and wind direction (d) as observed at the sugar-beet field of the KA site at the 13th of June, 1988. Wind speed was measured at 4 m above ground.

Abb. 7. Gemessene 30-Minuten-Mittel des Bodendrucks (a), der Globalstrahlung (b), der Windgeschwindigkeit (c) und der Windrichtung (d) über dem Zuckerrübenfeld der Karlsruher Station am 13.6.88. Die Windgeschwindigkeit wurde 4 m über Grund gemessen.

Table 5. Cluster analysis of land use distribution. Average (a) and maximum (m) cluster size is given in km.

Tabelle 5. Clusteranalyse der Landnutzungsverteilung. Mittlere (a) und maximale (m) Clustergröße in km.

	crops	beet	grass	villages	forest	water
a_{450}	1.2	0.6	0.5	0.5	0.6	0.3
m_{450}	2.1	1.0	0.8	0.7	0.8	0.3
a_{990}	2.0	1.2	0.7	0.7	0.7	0.0
m_{990}	2.5	1.6	1.0	0.8	0.8	0.0

$0.2\tau U$ in order to produce persistent secondary circulations. With $U \approx 4$m/s and the lifetime of secondary circulations $\tau \approx 1$ h, this gives a size of approximately 3 km. This agrees quite well with Shuttleworth, quoted in ANDRÉ et al. (1990), who estimated this extension to be in the order of 10 km. Looking at Table 5 and considering that crops, beet and grass produce similar heat fluxes and air temperatures, secondary circulations cannot be expected for the given land use distributions. Thus, we do not expect significant differences between the various simulations nor do we expect significant mesoscale contributions to the heat and moisture fluxes in the atmosphere. These expectations are fulfilled quite well as will be shown in the following.

We will consider the development and the properties of the PBL as simulated with the three-dimensional model with grid size 990 m (run L990). These results can be taken as representative for all of the simulations since no significant differences arose between runs L990, L450 and L0, thus verifying what was stated above.

Figure 8 shows the vertical profiles of the horizontally averaged potential temperature and specific humidity at 11:00, 14:00 and 18:00 CEST, together with the corresponding radiosonde and aircraft data. The simulated results are 10 minute averages centered as the respective time. At 11:00 CEST (Fig. 8 a) the potential temperature agrees well with the observations, whereas the specific humidity is predicted too high in the mixed layer by about 1.5 g/kg. The observed kink in the humidity in about 600 m above ground is not present in the simulations due to our smoothed initial data. At 14:00 CEST (Fig. 8 b) radiosonde data are only available from 800 m upward. Again the specific humidity is predicted higher than the aircraft data in the mixed layer and the temperature is overestimated above the mixed layer. The same is valid at 1800 CEST (Fig. 8 c). These differences can be partly attributed to warm air advection taking place during the afternoon and a corresponding increase in potential temperature (cf. Fig. 7). This synoptic process is not accounted for in the model, which assumes a steady basic state.

Figure 9 shows a plot of the calculated horizotal averages of potential temperature (a) and specific humidity (b) versus time. One can read off quite well the growth of the PBL and its moistening during the day. Figure 10 shows a plot of the horizontally averaged absolute potential temperature deviation at each level, defined as

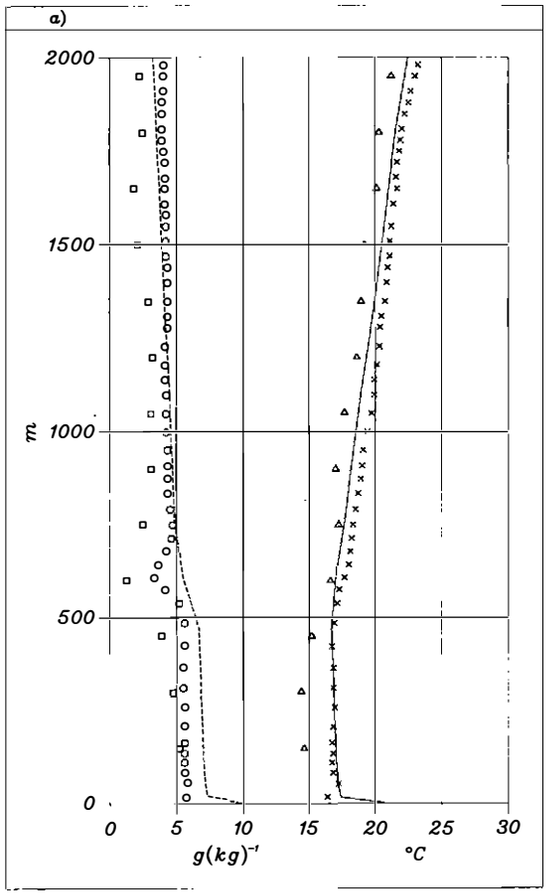

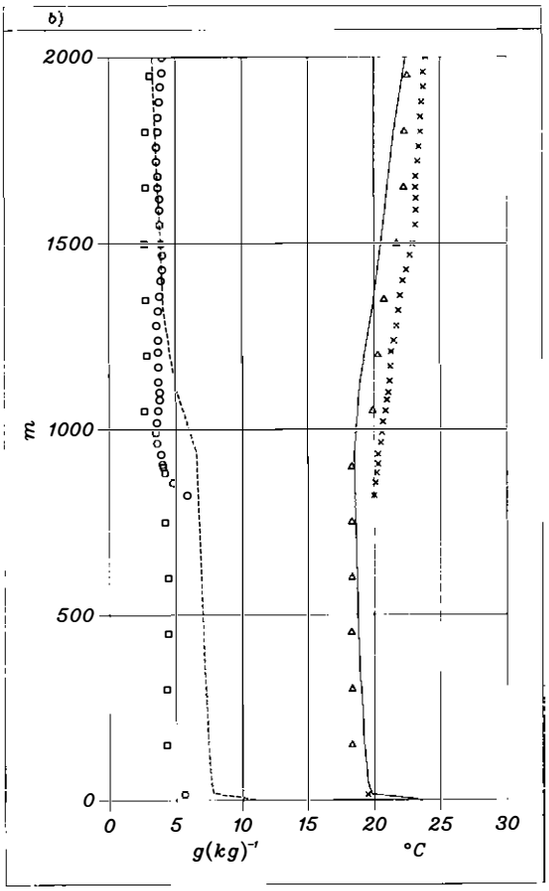

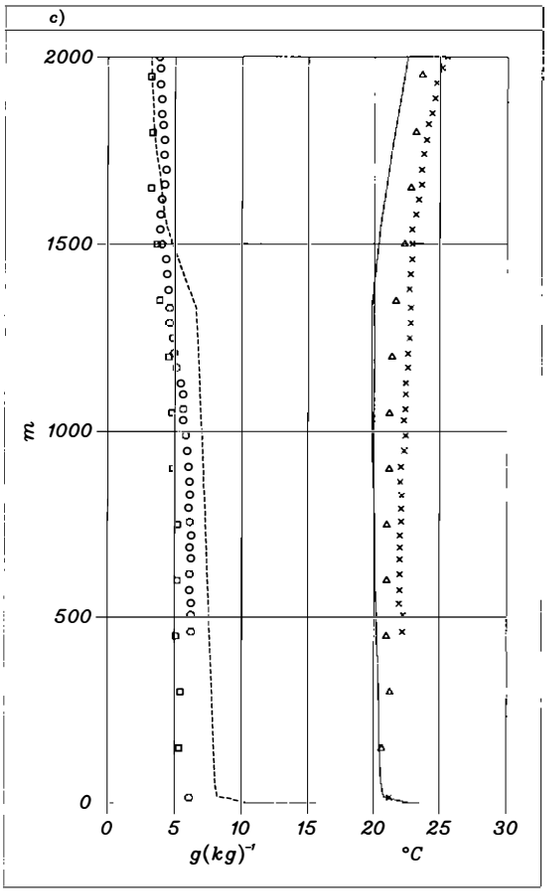

Fig. 8. Vertical profiles of horizontally averaged potential temperature (solid) and specific humidity (dashed) at 11:00 CEST (a), 14:00 CEST (b) and 18:00 CEST (c) at the 13th of June, 1988 obtained by L990. The corresponding radiosoundings are represented by crosses and circles, the corresponding aircraft data are given by squares and triangles, respectively.

Abb. 8. Vertikalprofile der horizontal gemittelten potentiellen Temperatur (durchgezogen) und spezifischen Feuchte (strichliert) um 11:00 MESZ (a), 14:00 MESZ (b) und 18:00 MESZ (c) für den 13.6.88 nach L990. Die entsprechenden Radiosondenwerte sind jeweils durch Kreuze und Kreise dargestellt, die Flugzeugdaten durch Quadrate und Dreiecke.

$$\Delta\Theta = \frac{1}{NX \times NY} \sum_{i=1}^{NX} \sum_{j=1}^{NY} |\Theta_{i,j} - \bar{\Theta}| \qquad (16)$$

where Θ is the potential temperature, $\bar{\Theta}$ is the horizontally averaged potential temperature and NX, NY are the number of grid points in the x- and y-direction, respectively. As could be expected the highest deviations occur in the lowest 50 metres above ground. Below this height horizonal inhomogeneities are not damped out, whereas above it the potential teperature field is smoothed out by horizontal advection and diffusion. A similar result is obtained for the specific humidity (not shown). These findings support the concept of the 'blending height' introduced by WIERINGA (1986) defined as the height where surface inhomogeneities are evened out. For the Netherlands he found a value of about 60 m.

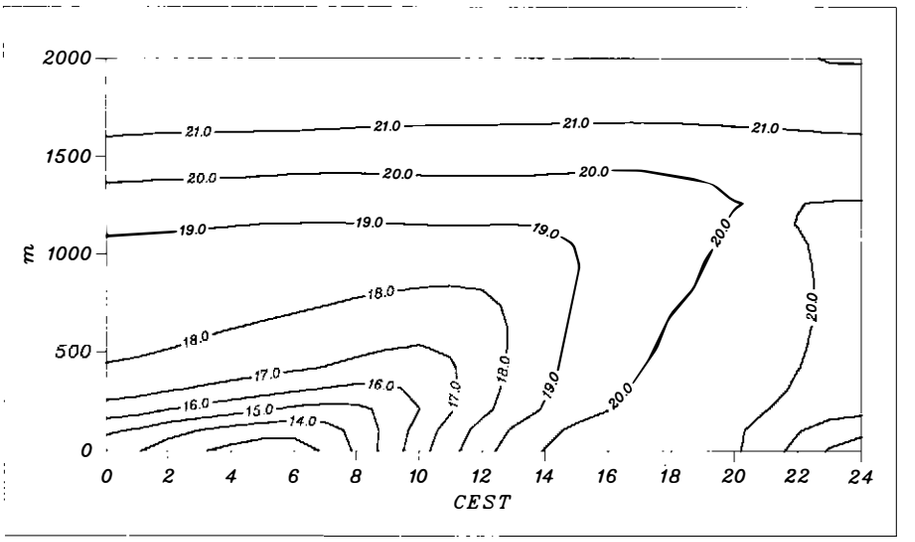

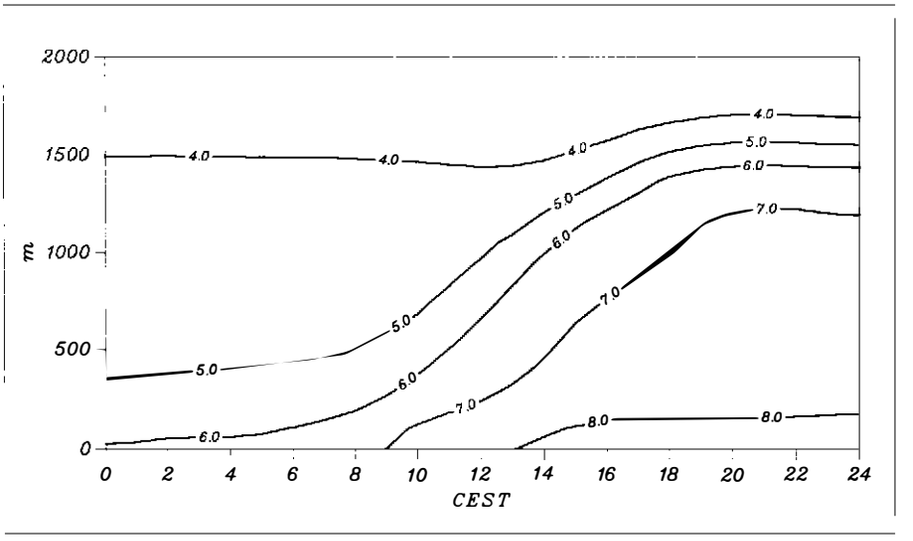

Fig. 9. Isopleths of horizontally averaged potential temperature in Celsius (top) and specific humidity in g/kg (bottom) for the 13th of June, 1988.

Abb. 9. Isoplethen der horizontal gemittelten potentiellen Temperatur in Celsius (oben) und spezifische Feuchte in g/kg (unten) für den 13.6.88.

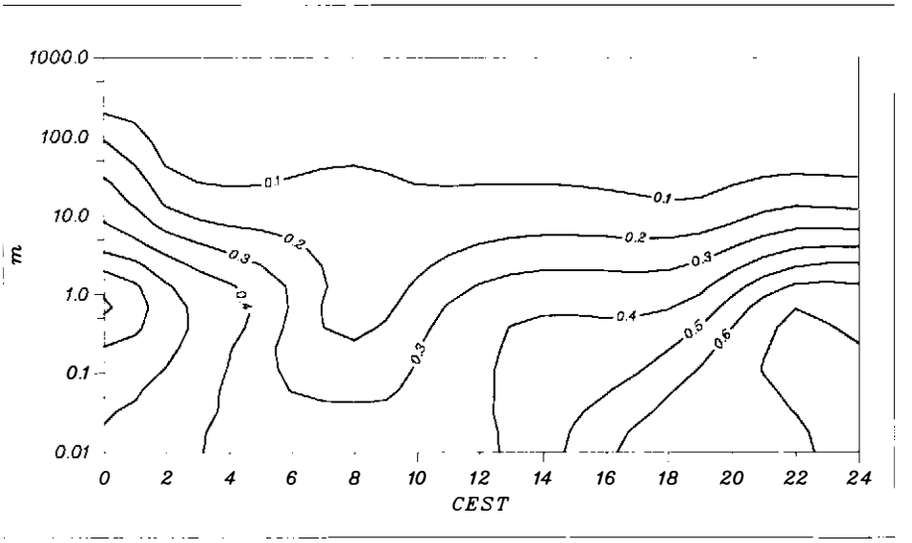

Fig. 10. Isopleths of horizontally averaged absolute potential temperature deviation in Celsius for the 13th of June, 1988.

Abb. 10. Isoplethen der horizontal gemittelten absoluten Abweichung der potentiellen Temperatur in Celsius für den 13.6.88.

Using a formula given by CLAUSSEN (1991) we obtained a blending height of about 90 m for a characteristic length of the horizontal variations of 2 km. Looking at Figure 10 the height at which the temperature deviation decreased to about 10 % of the surface value lies between 60 and 100 m.

Figure 11 shows a comparison of the sensible and latent heat fluxes between the model and the ones obtained from aircraft data for the times between 10:00—11:00 CEST, 13:00—14:00 CEST and 17:00—18:00 CEST. The observed fluxes are obtained during one hour over different flight legs (JOCHUM et al. 1991). Thus those data do not represent true area averages. To compare our model results with these fluxes we first calculated area averages and then averaged these over 60 minutes, centered at 10:30, 13:30 and 17:30, respectively. The comparison between the fluxes is difficult due to the scatter in the aircraft data. For the sensible heat flux, the agreement is generally better in the upper PBL whereas the latent heat fluxes agree better in the lower PBL. In general, the calculated heat fluxes are higher than the observed ones. Similar observations were made by BETTS et al. (1990) and ANDRÉ et al. (1990). The positions of the zeroes and minima, however, of the measured and the calculated sensible heat fluxes agree well thus indicating a coincidence between the measured anc calculated inversion heights. Taking the minimum of the sensible heat flux as a criterion for the PBL height (DEARDORFF 1974) we obtain values for the observed ($z_{i,obs}$) and calculated ($z_{i,calc}$) PBL heights listed in Table 6. As JOCHUM et al. (1991) indicate,

Table 6. Observed and calculated PBL heights.

Tabelle 6. Beobachtete und berechnete Grenzschichthöhen.

CEST	$z_{i,obs}$ (m)	$z_{i,calc}$ (m)
10:30	500	550
13:30	1000	1000
17:30	1300	1400

the observed fluxes depend on the maximum scale (minimum frequency) allowed (reducing the minimum frequency increases the flux) and the errors are between 20 an 30 % for the sensible heat flux and between 30 and 50 % for the latent heat flux. The profile of the sensible heat flux is 'standard" while the latent heat flux deviates quite a lot from the 'textbook profile' and somtimes attains its maximum within the mixed layer instead of the surface. Such behaviour shows up in observations (e. g. HECHTEL et al. 1990) and simulations (e. g. DEARDOFF 1973). MAHRT (1991) tried to classify several moisture regimes producing different latent heat flux profiles. It is a common experience that latent heat fluxes are much more difficult to measure and to simulate than sensible heat fluxes. Besides the large numerical value of the latent heat of evaporation, which strongly amplifies differences in the moisture-velocity correlation slight deviations in specific humidity can produce large deviations in the flux, and entrainment can change the profile completely. We expected that the fluxes would be the quantities to be influenced most by a change in grid size with respect to the partition between resolved fluxes and subgrid scale fluxes. Small grid sizes should give higher vertical velocities and thus could engender larger resolved scale fluxes. But again, our conjecture that due to the absence of large coherent regions of different land use no significant secondary circulations would appear, proved to hold: with the 990 m grid, the resolved scale fluxes were less than one percent of the total flux, whereas for the 450 m grid, the resolved scale fluxes amounted to a few percent of the total flux although the maximum vertical velocity for the 450 m grid was about five times higher than for the 900 m grid. The vertical velocities were about 5 times as high in run L450 compared to run L990.

In any case, we can state her that there is no significant difference between the two grid sizes and the one dimensional simulation.

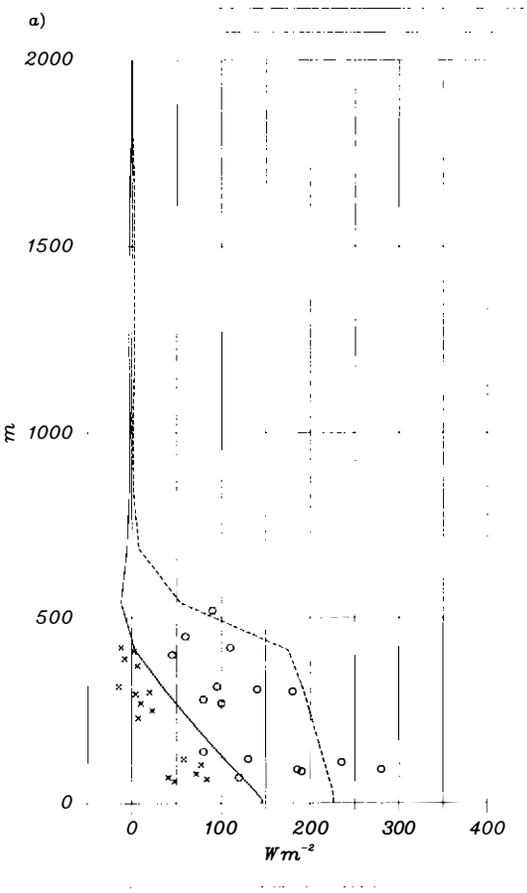

Fig. 11. Vertical profiles of horizontally averaged sensible (solid) and latent (dashed) heat flux at 10:30 CEST (a), 13:30 CEST (b) and 17:30 CEST (c) for the 13th of June, 1988. The corresponding aircraft data are represented by crosses (sensible heat flux) and circles (latent heat flux), respectively.

Abb. 11. Vertikalprofile des horizontal gemittelten fühlbaren (durchgezogen) und latenten (strichliert) Wärmeflusses um 10:30 MESZ (a), 13:30 MESZ (b) und 17:30 MESZ (c) für den 13.6.88. Die entsprechenden Flugzeugdaten sind durch Kreuze (sensibler Wärmestrom) und Kreise (latenter Wärmestrom) dargestellt.

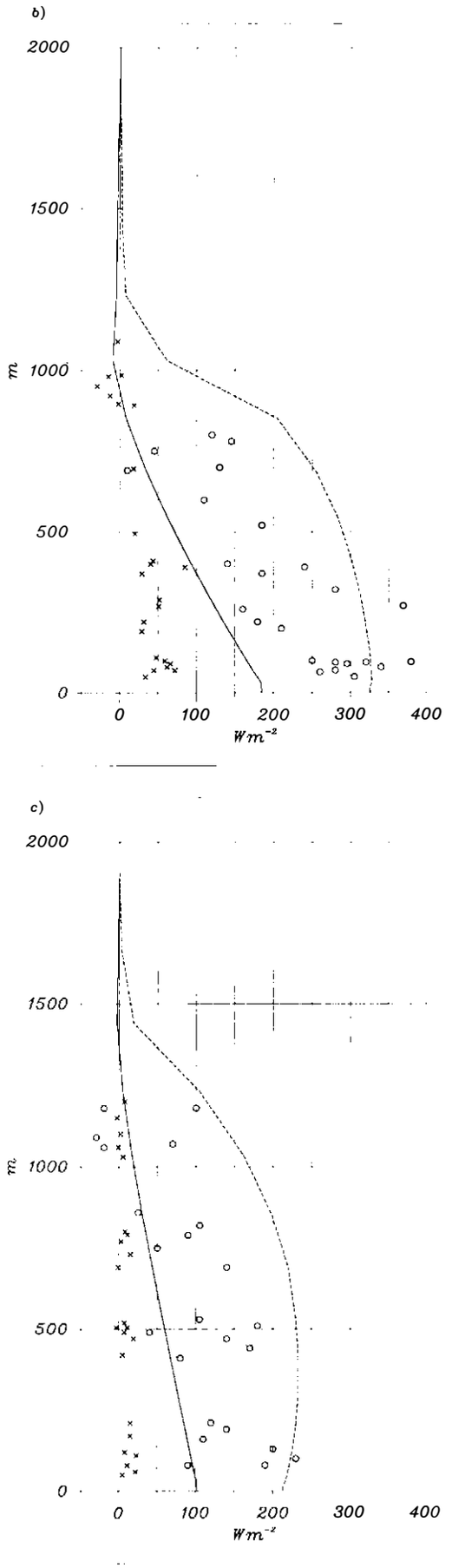

Fig. 11. (cont.)

Abb. 11. (Fortsetzung)

4.2 Radiation temperatures and surface energy balances

In this section we will intercompare model results of the energy balance components of the different model runs (L0, L450 and L990) as well as the model results for the 990 m grid with point measurements. The data of the model results wer chosen from the nearest gridpoint of the measurements, done at KA. The values of the turbulent fluxes were calculated by the aerodynamic method (I), as described in section 2.

The turbulent surface fluxes and radiation temperatures for the different land use classes are shown in Figure 12 to Figure 16. It can be seen that the model results agree quite well for the sugar-beet field. Concerning the wheat field two things can be stated. Firstly, the stimulated sensible heat is higher than measured at the different sites of Karlsruhe and Braunschweig. Measurements of the sensible heat flux by the eddy-correlation method by the group of Berlin (BLÜMEL et al. 1989), too, (for the same day, but outside the model domain) yield about 100—120 W m^{-2} at noon. Secondly, the modelled latent heat flux is within the range of the observations. The local differences, however, are very high. This could be caused by a different state of the crops, different soil moisture content and different microclimatic conditions between the sites of KA and BS.

The turbulent fluxes for the remaining land uses are shown in the Figures 14, 15 and 16. It can be seen that especially the forest and the villages differ very much from the other kinds of vegetation (wheat, grass and sugar beets). For the forest the sensible and latent heat flux are of the same order (the sensible heat flux dominates before noon, while the latent heat flux is higher during the afternoon), while within villages the net radiation is transformed into the sensible (about 75 %) and soil heat flux (about 25 %). The contribution of the latent heat flux is nearly negligible.

The surface temperatures over the different kinds of crops are shown in the right part of the Figures 12 to 16. It can be seen that the temperatures of the wheat field and the forest are the lowest with a maximum value of 25 °C. Measurements of the group of Braunschweig of the surface temperature give a maximum value of 26.2 °C for barley, 24.2 °C for wheat and 24.3 °C for rye. This indicates the range of the temperature of the different kinds of crops and fits well with the model results and the observation made at KA. Measurements of the group of Braunschweig over a sugar-beet field yield a maximum temperature of 27.7 °C, which also confirms the model results obtained at the sugar beets. For the results predicted for the forest, grass and village no mesurements are available. However, own comparisons of measured and modelled energy balances of a forest at a different site (EBERT, Institut für Meteorologie und Klimaforschung/Universität Karlsruhe, personal communication, 1991) make the results reliable.

Recently evaporation calculations have been published by LÖPMEIER (1991) for the time interval from 12:00 to 13:00 CEST of June 13, 1988. The calculation of the evaporation is based on the Penman-Monteith formula coupled with a soil water model. The results for the different land

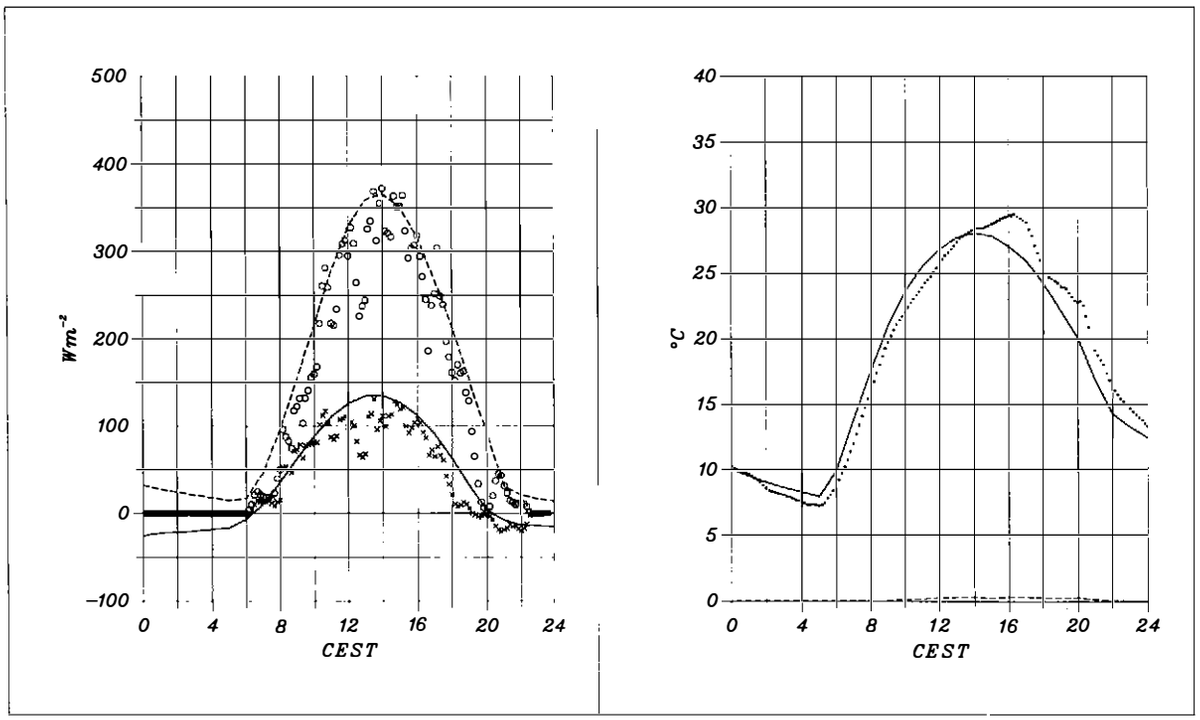

Fig. 12. Left: Comparison of calculated and measured turbulent fluxes for sugar beet for the 13th of June, 1988. Solid: calculated sensible heat flux, crosses: measured sensible heat flux at KA site; dashed: calculated latent heat flux, circles: measured latent heat flux at KA site. Right: Comparison of calculated (solid) and measured (dotted) radiation temperatures at KA site. The dashed line indicates the standard deviation from the model results.

Abb. 12. Links: Vergleich von berechneten und gemessenen Wärmeflüssen über Zuckerrüben. Durchgezogen: berechneter fühlbarer Wärmefluß, Kreuze: gemessener fühlbarer Wärmefluß an der Karlsruher Station; strichliert: berechneter latenter Wärmefluß, Kreise: gemessener latenter Wärmefluß an der Karlsruher Station. Rechts: Vergleich von berechneten (durchgezogen) und gemessenen (punktiert) Strahlungstemperaturen an der Karlsruher Station. Die gestrichelte Kurve gibt die Standardabweichung für die Modellrechnungen an.

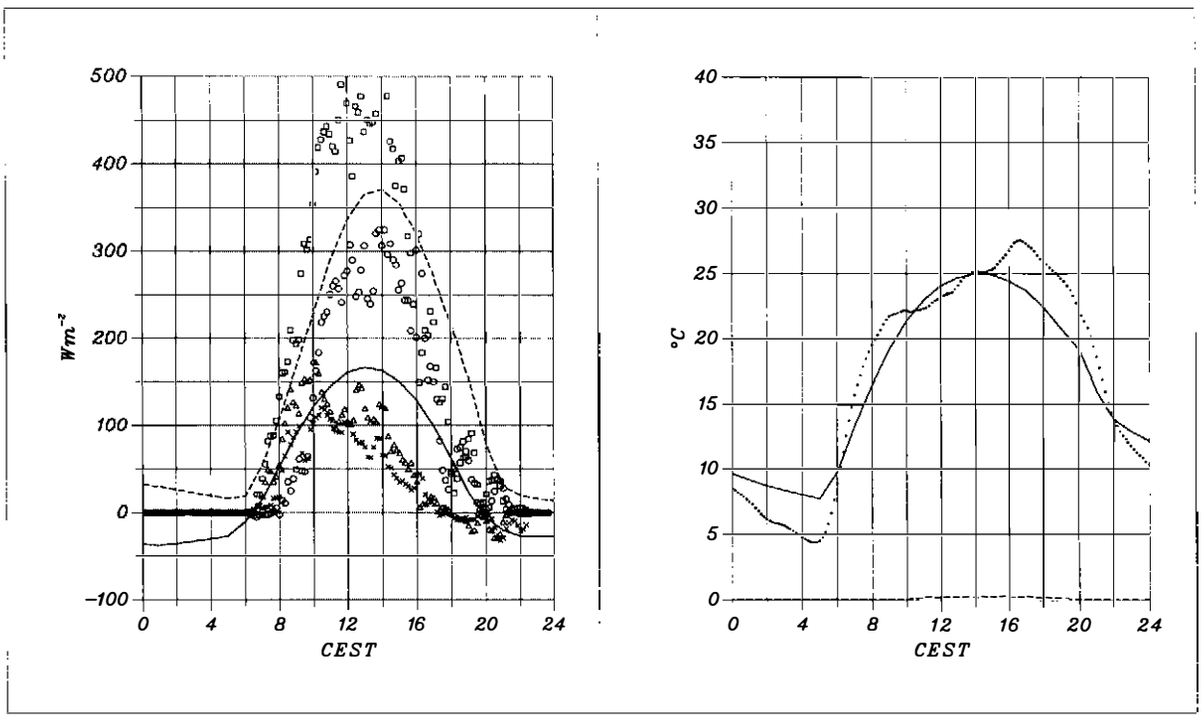

Fig. 13. Left: Comparison of calculated and measured turbulent fluxes for wheat for the 13th of June, 1988. Solid: calculated sensible heat flux, crosses: measured sensible heat flux at KA site, triangles: measured sensible heat flux at BS site; dashed: calculated latent heat flux, circles: measured latent heat flux at KA site, squares: measured latent heat flux at BS site. Right: Comparison of calculated (solid) and measured (dotted) radiation temperatures at KA site.

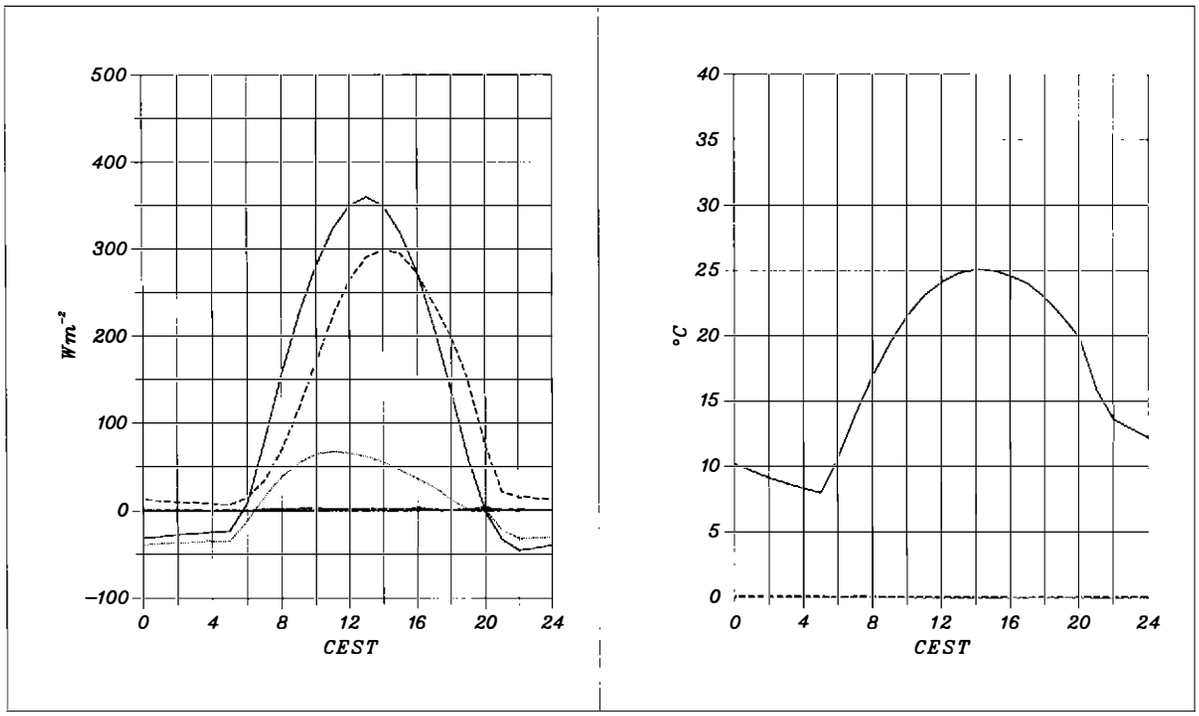

Fig. 14. Left: calculated energy fluxes for forest for the 13th of June, 1988. Solid: sensible heat flux, dashed: latent heat flux, dotted: soil heat flux; dot-dashed: standard deviation of sensible heat flux, short/long-dashed: standard deviation of latent heat flux, very short-dashed: standard deviation of soil heat flux. Right: radiation temperature for forest.

Abb. 14. Links: berechnete Energieflüsse über Wald für den 13.6.88. Durchgezogen: fühlbarer Wärmefluß, strichliert: latenter Wärmefluß, punktiert: Bodenwärmestrom; strichpunktiert: Standardabweichung des fühlbaren Wärmeflusses, kurz-lang strichliert: Standardabweichung des latenten Wärmeflusses, kurz strichliert: Standardabweichung des Bodenwärmestroms. Rechts: Strahlungstemperatur für Wald.

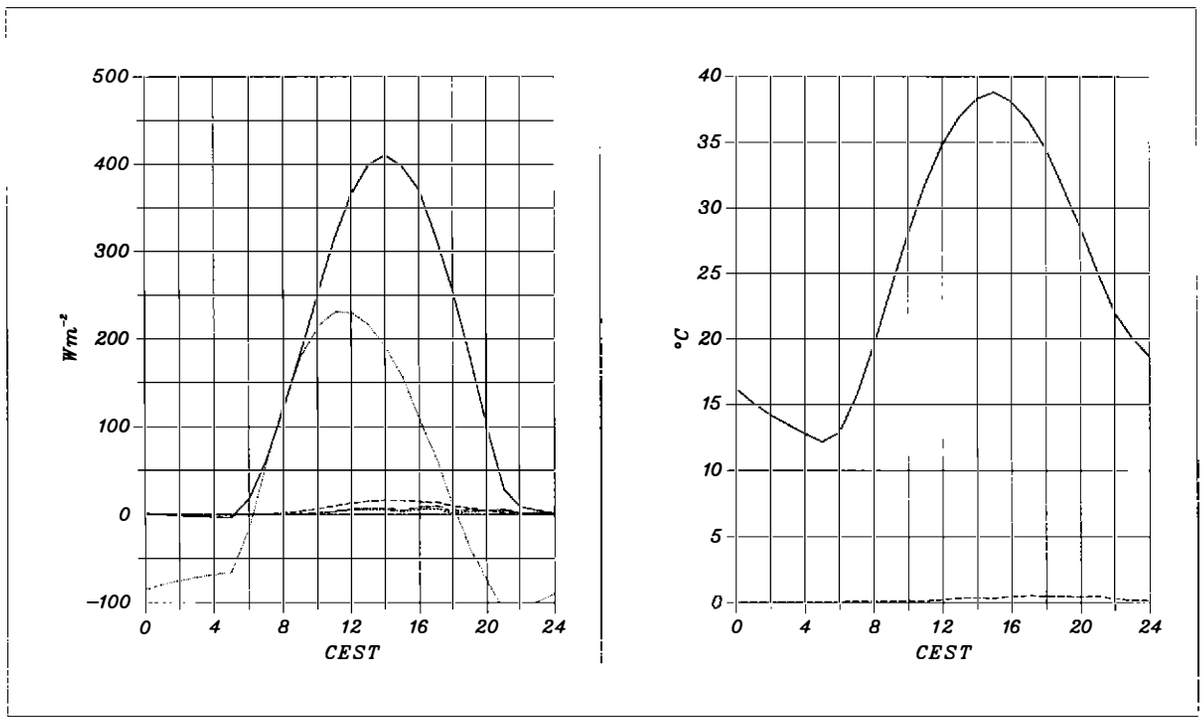

Fig. 15. Same as Figure 14 but for villages.

Abb. 15. Wie Abb. 14, aber für besiedeltes Gebiet.

◁ Abb. 13. Links: Vergleich von berechneten und gemessenen Wärmeflüssen über Weizen für den 13.6.88. Durchgezogen: berechneter fühlbarer Wärmefluß, Kreuze: gemessener fühlbarer Wärmefluß an der Karlsruher Station, Dreiecke: gemessener fühlbarer Wärmefluß an der Braunschweiger Station, strichliert: berechneter latenter Wärmefluß, Kreise: gemessener latenter Wärmefluß an der Karlsruher Station, Quadrate: gemessener latenter Wärmefluß an der Braunschweiger Station. Rechts: Vergleich von berechneten (durchgezogen) und gemessenen (punktiert) Strahlungstemperaturen an der Karlsruher Station.

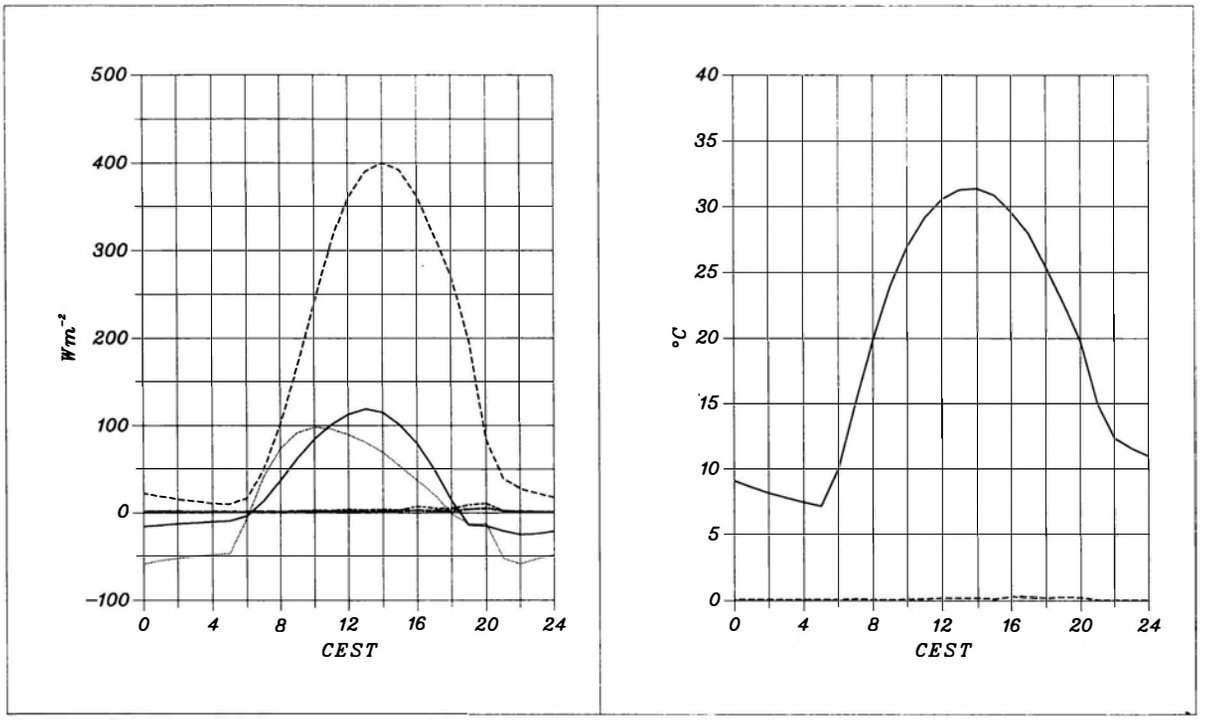

Fig. 16. Same as Figure 14 but for grass.

Abb. 16. Wie Abb. 14, aber für Gras.

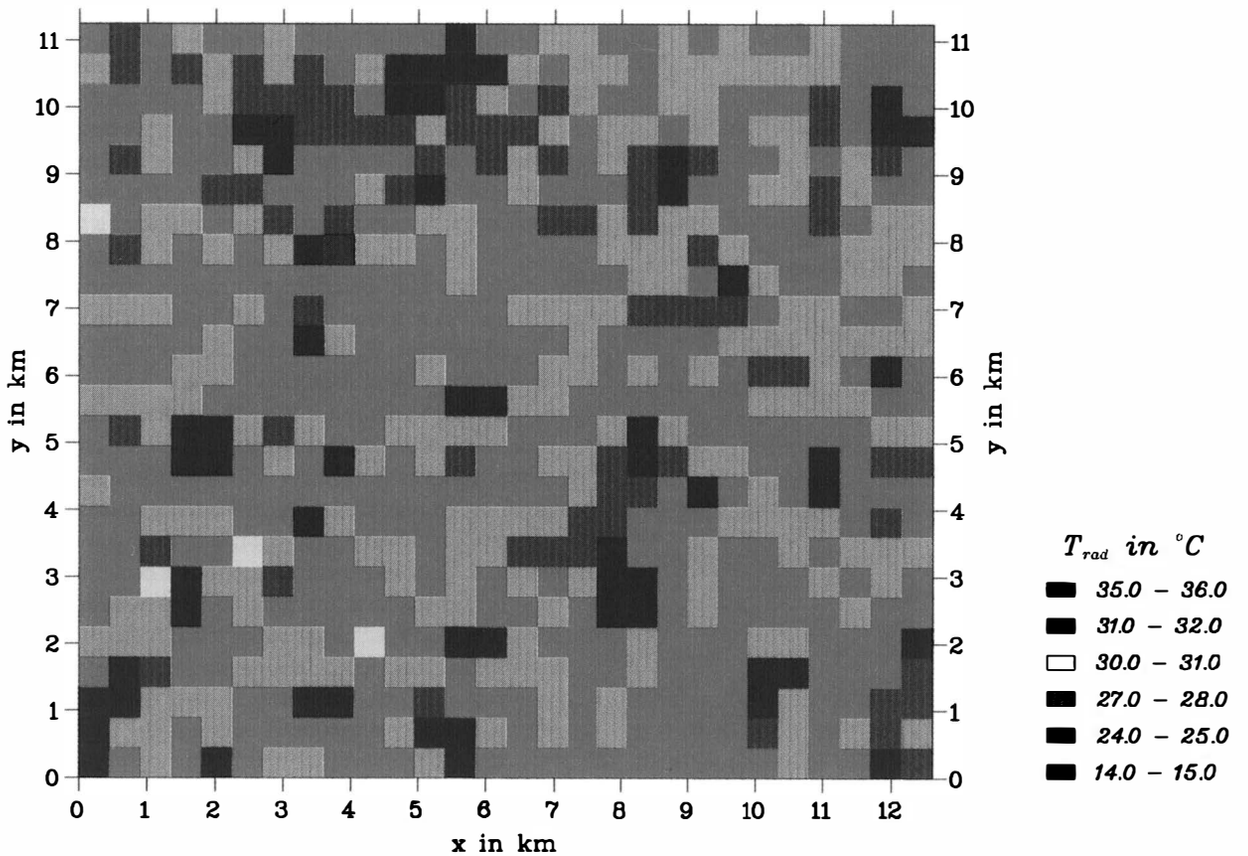

Fig. 17. Calculated radiation temperatures for the 13th of June, 1988 at 12:00 CEST for the 450 m grid.

Abb. 17. Berechnete Strahlungstemperaturen für den 13.6.88 um 12:00 Uhr MESZ für das 450 m-Gitter.

Table 7. Evaporation for different land use classes of the HIBE area for the 13th of June, 1988 from 12.00 to 13.00 CEST.

Tabelle 7. Verdunstungsrate der verschiedenen Landnutzungsklassen in der Hildesheimer Börde für den 13.6.88 von 12:00 bis 13:00 MESZ.

land use class	LÖPMEIER	KAMM results
crops	0.52	0.51
beet	0.50	0.50
grass	0.49	0.54
forest	0.53	0.41
village	0.05	0.02

use classes are summarized in Table 7. The data agree well for crops and sugar beets, whereas for grass, forests and villages noticeable differences can be found. However, as those land use classes are of minor importance in the whole HIBE area the areally-averaged evaporation (i.e. the individuel evaporation weighted by the corresponding percentage land use coverage) from LÖPMEIER (0.53 mm/h) and our own calculations (0.50 mm/h) only differ by 6 %.

Figure 17 shows the calculated radiation temperatures at 12:00 CEST for the whole modelling area as obtained with the 450 m grid. Due to the small standard deviations within a land use class, the map of the radiation temperatures reflects the land use map shown in Figure 3.

Figure 18 now gives the areally-averaged fluxes for the whole model area. It can be stated that the main energy is

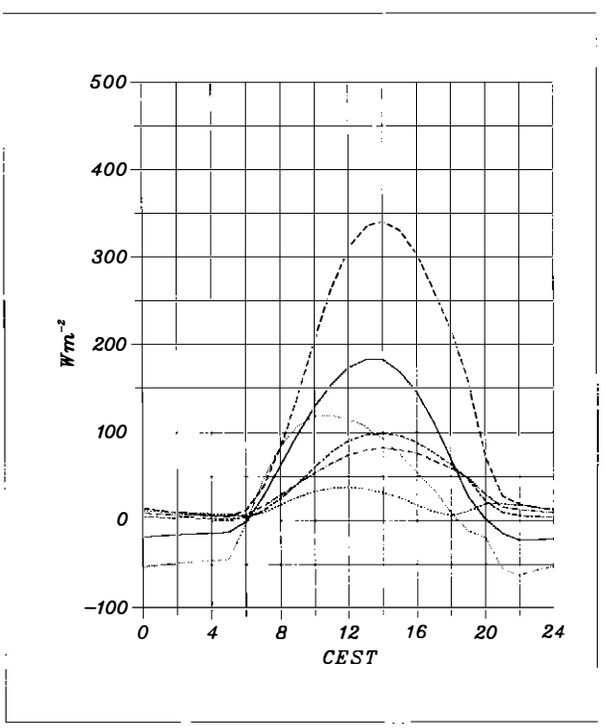

Fig. 18. Area averages of the components of the energy balance for the whole simulation domain for the 13th of June, 1988 and corresponding standard deviations. Legend as for Figure 14.

Abb. 18. Flächenmittel der Energiebilanzkomponenten vom 13.6.88 für das gesamte Simulationsgebiet und zugehörige Standardabweichungen. Legende wie bei Abb. 14.

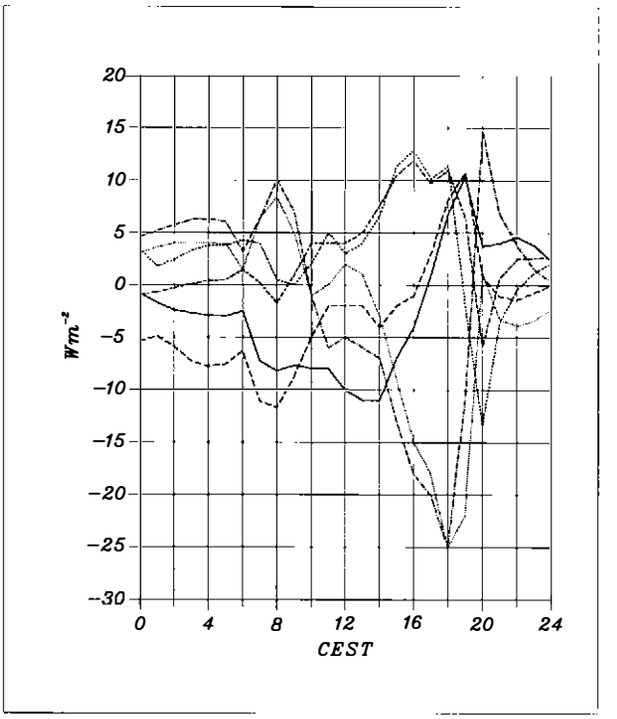

Fig. 19. Comparison of the energy balance components between the three model runs (L0, L450 and L990): The solid line indicates H(L0) — H(L990), the dashed line indicates H(L450) — H(L990), the dotted line gives E(L0) — E(L990), the dashed-dotted line gives E(L450) — E(L990), the long short-dashed line gives B(L0) — B(L990) and the short-dotted line give B(L450) — B(L990).

Abb. 19. Vergleich der Energiebilanzkomponenten aus den verschiedenen Rechenläufen (L0, L450 and L990): Die durchgezogene Linie kennzeichnet H(L0) — H(L990), die gestrichelte H(L450) — H(L990), die gepunktete E(L0) — E(L990), die strichpunktierte E(L450) — E(L990), die lang und kurz gestrichelte B(L0) — B(L990) und die kurz gestrichelte B(L450) — B(L990).

transformed into latent heat (about 350 Wm^{-2} at noon), while the sensible heat flux reaches about 190 Wm^{-2} at noon. This is in accordance with the dominating land use being crops and sugar beets and their energy balance. Additionally the standard deviation of the different components of the energy balance is shown. For both the latent and sensible heat flux they reach about 100 Wm^{-2} at noon. These high standarad deviations result from the totally different behavior of the energy transformation of the villages and forests. Figure 19 finally gives the differences for the energy balance components between the L0 and L450 model runs and the L990 run. Generally these differences are less than 10 Wm^{-2} for H, E and the soil heat flux B (i. e. less than 10 % at noon), except for the latent heat flux in the afternoon.

5 Conclusions

The objectives of this investigation are to estimate areally-averaged energy balances of the grid size of satellite pictures and for the whole Hildesheimer Börde for the HIBE88

campaign. This was achieved with the three-dimensional mesoscale model KAMM coupled with a soil-vegetation model. The model results were compared (i) with the turbulent fluxes measured over different surfaces (sugar beets and wheat) and (ii) with the vertical distribution of the potential temperature and humidity fields as measured by the radiosonde and aircraft and (iii) with the BPL-profiles of the turbulent fluxes as been obtained by aircraft data.

The model results generally are in agreement with the observed data. The difference between the modelled and the measured daily evaporation for the wheat and sugar-beet fields is about 15 %. The differences between the calculated and measured boundary layer heights are less than 10 %.

Furthermore from the model results some additional informations can be received: A main feature of the Hildesheimer Börde is that there are no secondary induced circulations, i. e. the grid size of the model is of minor importance. This is caused by (i) the weak differences between the vegetations and (ii) by the small size of the land used areas (the mean size is generally less than 2 km). Finally a 'blending height' can be estimated from the temperature and humidity fields, which lies, independent of the stability, between 50 and 100 m.

The results obtained here now can be used for different purposes: (i) to test and improve appropriate averaging procedures for one-dimensional models, (ii) to deliver area averages for algorithms (e. g. LÖPMEIER 1991 and BECKER et al. 1988) which estimate turbulent fluxes (generally evaporation) from radiation intensities received from satellite data.

The experience gained here is useful for future modelling purposes, too. For instance, large scale processes, if present, should be somehow incorporated in the model. This would account for the differences between modelled and observed potential temperature above the boundary layer in the afternoon. The difference between the fluxes in the atmosphere as derived from aircraft data and the ones calculated by the model await further investigation. This concerns the method of obtaining the fluxes from aircraft measurements as well as their calculation with a numerical model. Thirdly, great care has to be put into the initialisation of the model. It seems that the average specific humidity near the surface is predicted too high by the model. This could be due to unrealistic soil moisture values for the land use classes where no data were available (especially grassland and forest) and perhaps unappropriate prescription of soil and vegetations parameters.

Acknowledgement

We like to thank O. WALK for providing the radiosonde data, G. KLINCK for plotting most of the drawings and S. UNGEHEUER for doing the administrative tasks of the projekt. Furthermore, we thank the other groups participating in the LOTREX experiment, especially A. BEBLIK, M. WEGEHENKEL and A. JOCHUM, for providing land use, soil moisture and aircraft data, and Prof. R. ROTH for the coordination of the project. The LOTREX-10E subprogramme was supported by the "Bundesministerium für Forschung und Technologie" (FRG), under contract number LOF 43/87.

References

Adrian, G., F. Fiedler, 1991: Simulation of unstationary wind- and temperature fields over complex terrain and comparison with observations. — Beitr. Phys. Atmosph. **64**, 27—48.

André, J.-C., P. Bougeault, J.-P. Goutorbe 1990: Regional estimates of heat and evaporation fluxes over non-homogeneous terrain. Examples from the HAPEX-MOBILHY programme. — Bound. Lay. Meteorol. 50, 77—108.

André, J.-C., J.-P. Goutorbe, A. Perrier, F. Becker, P. Bessemoulin, P. Bougeault, Y. Brunet, W. Brutsaert, T. Carlson, R. Cuenca, J. Gash, J. Gelpe, P. Hildebrand, J.-P. Lagouarde C. Lloyd, L. Mahrt, P. Mascart, C. Mazaudier, J. Noilhan, C. Ottlé, M. Payen, T. Phulpin, R. Stull, J. Shuttleworth, T. Schmugge, O. Taconet, C. Tarrieu, R.-M. Thepenier, C. Valencogne, D. Vidal-Madjar, A. Weill, 1988: Evaporation over land-surfaces: First results from HAPEX-MOBILHY special observing period. — Ann. Geophys. 6, 477—492.

Atwater, M. A., P. S. Brown, 1974: Numerical calculation of the latitudinal variation of solar radiation for an atmosphere of varying opacity. — J. Appl. Meteorol. **13**, 289—297.

Becker, F., H.-J. Bolle, P. R. Rowntree, 1988: The international satellite land-surface climatology project. — ISLSCP-Rep. No. 10, 100 pp.

Beljaars, A. C. M. and A. A. M. Holtslag, 1991: Flux parameterization over land surfaces for atmospheric models. — J. Appl. Meteorol. 30, 327—341.

Betts, A. K., R. L. Desjardins, J. I. Macpherson, R. D. Kelly, 1990: Boundary-layer heat and moisture budgets from FIFE. — Bound. Lay. Meteorol. 50, 109—137.

Biggs, W. G., Graves, M. E. 1962: A Lake Breeze Index. — J. Appl. Meteorol. 1, 474—480.

Blümel, K., Eckhardt M., Wohlfart, U., Bolle J.-J. 1989: Ableitung von Landoberflächen-Daten aus Satellitenmessungen, ihre Validierung und Nutzung in der Klimamodellierung. — In: Klimaforschungsprogramm. Statusseminar 10.01.— 12.01.1989, Ed. Gesellschaft für Strahlen- und Umweltforschung, 175—178.

Businger, J. A., J. C. Wyngaard, Y. Izumi, E. F. Bradley, 1971: Flux profile relationships in the atmospheric surface layer. — J. Atmos. Sci. 28, 181—189.

Clapp, R. B., G. M. Hornberger, 1978: Empirical equations for some soil hydraulic properties. — Water Resources Res. 14, 601—604.

Claussen, M., 1991: Estimation of areally-averaged surface fluxes. — Bound. Lay. Meteorol. 54, 387—410.

Deardorff, J. W., 1973: Three-dimensional numerical modeling of the planetary boundary layer. — In: Workshop on Micrometeorology, Ed. D. A. Haugen. Amer. Meteorol. Soc., Boston, 392 pp.

— 1974: Three-dimensional numerical study of the height and mean structure of a heated planetary boundary layer. — Bound. Lay. Meteorol. 7, 81-106.

Dickinson, R. E., A. Henderson-Sellers, P. J. Kennedy, M. F. Wilson, 1986: Biosphere-atmosphere transfer scheme (BATS) for the NCAR community climate model. — NCAR Technical Note NCAR/TN-275+STR., Boulder.

Fiedler, F., H. A. Panofsky, 1972: The geostrophic drag coefficient and the effective roughness length. — Q. J. Roy. Meteorol. Soc. 98, 213—220.

Gould, H., J. Tobochnik, 1988: An Introduction to Computer Simulation Methods. — Addison-Wesley, Reading, 695 pp.

Graf, J., U. Schumann, 1991: Simulation der konvektiven Grenzschicht im Vergleich mit Flugzeugmessungen beim LOTREX-Experiment — Meteorol. Rdsch. **43**, 140—148.

Hanna, S. R., 1987: An empirical formula for the height of the coastel internal boundary layer. — Bound. Lay. Meteorol. 40, 205—207.

Hechtel, L. M., C.-H. Moeng, R. B Stull, 1990: The effects of nonhomogeneous surface fluxes on the convective boundary layer: A case study using large-eddy simulation. — J. Atmos. Sci. **47**, 1721—1741.

Hoppmann, U., J. Hoffmann, 1991: Die Feldexperimente HIBE '88 und '89. — In: Experimentbericht zu den Feldexperimenten HIBE '88 und '89, Eds. U. Hoppmann and R. Roth, Ber. Inst. Meteorol. Klimatol. T. U. Hannover, B2, 4—8.

Hoshen, J., R. Kopelman, 1976: Percolation and cluster distribution. I. Cluster multiple labeling technique and critical concentration algorithm. — Phys. Rev. **B14**, 3438.

Houghton, J. T., 1979: The Physics of Atmospheres. — Cambridge University Press, London.

Jacquemin, B., J. Noilhan, 1990: Sensitivity study and validation of a land surface parameterization using the HAPEX-MOBILHY data set. — Bound. Lay. Meteorol. **52**, 93—134.

Jochum, A. M., R. Baumann, D. Baumgardner, N. Entstrasser, H. P. Fimpel, J. Lidl, V. Machmeier, P. Mörl, D. Paffrath, F. Rösler, S. Schulz, H. Willeke, R. Schmidt, 1991: Flugzeugmessungen in der atmosphärischen Grenzschicht für Fragen der Wechselwirkung Atmosphäre-Landoberfläche. — In: Experimentbericht zu den Feldexperimenten HIBE '88 und '89, Eds. U. Hoppmann and R. Roth, Ber. Inst. Meteorol. Klimatol. T. U. Hannover, B2, 221—234.

Kalthoff, N., U. Corsmeier, F. Fiedler, 1991: Modification of turbulent fluxes and temperature fields in the atmospheric surface layer over two adjacent agricultural areas: a case study. — Ann. Geophys. **9**, 521—533.

Linse, A., G. Tetzlaff, 1991: Einfluß von Inhomogenitäten des Untergrundes auf den Wärmehaushalt der Oberfläche. — In: Experimentbericht zu den Feldexperimenten HIBE '88 und '89, Eds. U. Hoppmann and R. Roth, Ber. Inst. Meteorol. Klimatol. T. U. Hannover, B2, 118—156.

Löpmeier, F.-J., 1991: Die Bestimmung der realen Evapotranspiration unter besonderer Berücksichtigung von Fernerkundungsmethoden. — Beitr. Agrarmeteorol. Nr. 6/91. Deutscher Wetterdienst, Offenbach/Main, 98 pp.

Löpmeier, F.-J., A. J. Beblik, S. Schröder, 1991: Fernerkundungsdaten für agroklimatologische Zwecke. Verdunstungsbestimmung mittels Fernerkundung. — In: Experimentbericht zu den Feldexperimenten HIBE '88 und '89, Eds. U. Hoppmann and R. Roth, Ber. Inst. Meteorol. Klimatol. T. U. Hannover, B2, 65—90.

Mahrt, L., 1987: Grid-averaged surface fluxes. — Month. Weath. Rev. **115**, 1550—1560.

— 1991: Boundary-layer moisture regimes. — Q. J. Roy. Meteorol. Soc. **117**, 151—176.

Mason, P. J., 1988: The formation of areally-averaged roughness lengths. — Q. J. Roy. Meteorol. Soc. **114**, 432—440.

Neumann, P., G. A. Schultz, 1991: Eichung und Validierung von Satellitendaten zu gebietsspezifischen Parametern hydrologischer Modelle. — In: Experimentbericht zu den Feldexperimenten HIBE '88 und '89, Eds. U. Hoppmann and R. Roth, Ber. Inst. Meteorol. Klimatol. T. U. Hannover, B2, 59—64.

Nieuwstadt, F., 1978: The computation of the friction velocity u_* and the temperatur scale T_* from temperature and wind velocity profiles by least-square methods. — Bound. Lay. Meteorol. **14**, 235—246.

Oke, T. R., 1987: Boundary layer climates, 2nd ed. — Methuen and Co., Ltd., London U.K., 435 pp.

Pan, H.-L., L. Mahrt, 1987: Interaction between hydrology and boundary-layer development. Bound. Lay. Meteorol. **38**, 185—202.

Rösler, F., A. M. Jochum, 1988: Tagesgang der atmosphärischen Grenzschicht während LOTREX/HIBE 88, Datenband 3: Umweltmeßflugzeug Queen Air. — DLR IB 553-88/19, 79 pp.

Schädler, G., 1990: Numerische Simulationen zur Wechselwirkung zwischen Landoberflächen und atmosphärischer Grenzschicht. — Wiss. Ber. Inst. Meteorol. Klimaf. Univ. Karlsruhe, Nr. 13.

Schädler, G., N. Kalthoff, F. Fiedler, 1990: Validation of a model for heat, mass and momentum exchange over vegetation surfaces using LOTREX-10E/HIBE88 data. — Beitr. Phys. Atmosph., **63**, 85—100.

Sellers, P. J., F. G. Hall, G. Asrar, G. Strebel, R. E. Murphy, 1988: The First ISLSCP field experiment (FIFE). — Bull. Amer. Meteorol. Soc. **68**, 22—27.

Staley, D. O., G. M. Jurica, 1970: Flux emissivity tables for water vapor, carbon dioxide and ozone. — J. Appl. Meteorol. **9**, 365—372.

Vihma, T., H. Savijärvi, 1991: On the effective roughness length for heterogeneous terrain. — Q. J. Roy. Meteorol. Soc. **117**, 399—407.

Wegehenkel, M., W. Mauser, 1991: Messungen zur Erfassung der Bodenwasserbilanz im Untersuchungsgebiet von HIBE mit besonderer Berücksichtigung des Feuchteverlaufs an der Bodenoberfläche und in den oberflächennahen Bodenkompartimenten im Rahmen der HIBE '88 u. '89 Kampagnen. — In: Experimentbericht zu den Feldexperimenten HIBE '88 und '89, Eds. U. Hoppmann and R. Roth, Ber. Inst. Meteorol. Klimatol. T. U. Hannover, B2, 91—117.

Weill, A., C. Mazaudier, F. Baudin, C. Klapisz, F. Leca, M. Masmoudi, D. Vidal Madjar, R. Bernard, O. Taconet, B. S. Gera, A. Sauvaget, A. Druilhet, P. Durand, J. Y. Caneil, P. Mery, G. Dubosclard, A. C. M. Beljaars, W. A. A. Monna, J. G. Van der Vliet, M. Crochet, D. Thomson, T. Carlson, 1988: The 'MESOGERS 84' experiment: a report. — Bound. Lay. Meteorol. **42**, 251—264.

Wieringa, J., 1986: Roughness-dependent geographical interpolation of surface wind speed averages. — Q. J. Roy. Meteorol. Soc. **112**, 867—889.

Wilson, M. F., A. Henderson-Sellers, R. E. Dickinson, P. J. Kennedy, 1987: Sensitivity of the biosphere-atmosphere transfer scheme (BATS) to the inclusion of variable soil characteristics. — J. Climate Appl. Meteorol. **26**, 341—362.

Address of the responsible author:
Dr. N. KALTHOFF
Institut für Meteorologie
und Klimaforschung
Kernforschungszentrum
Karlsruhe GmbH/
Universität Karlsruhe
Postfach 3640
W-7500 Karlsruhe 1
Germany

Received: 26. 1. 1992, accepted: 21. 6. 1992